R. & M. No. 2938
(16,172)
(A.R.C. Technical Report)

MINISTRY OF SUPPLY

AERONAUTICAL RESEARCH COUNCIL
REPORTS AND MEMORANDA

An Experimental Investigation of the Effects of Deformation on the Aerodynamic Characteristics of a Swept-back Wing

By

JOSEPH BLACK, Ph.D.,

University of Bristol,
Department of Aeronautical Engineering

LONDON: HER MAJESTY'S STATIONERY OFFICE

1956

NINE SHILLINGS NET

An Experimental Investigation of the Effects of Deformation on the Aerodynamic Characteristics of a Swept-back Wing

By

JOSEPH BLACK, Ph.D.,

University of Bristol,
Department of Aeronautical Engineering

Reports and Memoranda No. 2938

September, 1953

Summary.—A wind-tunnel investigation of the effects of structural deformation on the pressure distributions round a tapered wing, with 44-deg leading-edge sweepback, has been carried out over a range of deformations at a Reynolds number of $0{\cdot}6 \times 10^6$.

A technique for constructing a model and deforming it into any desired deformation has been successfully developed. The model is made of Perspex which becomes plastic at 100 deg C.; after being boiled in a water bath the model can be deformed into any desired deformation, and on cooling, it sets hard with the deformation 'frozen' in. When the model is boiled again it reverts to its undeformed shape and a new deformation can then be applied while it is in its plastic state. The cycle can be repeated any number of times with the same model, to cover a range of deformations.

From the modes investigated the appropriate deformations required to produce an almost elliptic span loading at a selected moderate overall lift, or to delay tip stalling at high incidence, were established. The most important feature is to have a maximum wash-out at about $0{\cdot}7$ semi-span, with a decrease of wash-out from there to the tip, and not a continuously increasing wash-out right to the tip.

The Weissinger method for theoretical prediction of airloads was found to be reasonably satisfactory for the effect of deformation at low incidence.

LIST OF SYMBOLS

b		Span
c		Section chord
c_{av}	$=$	S/b, wing average chord
$\bar{c}$	$=$	$\dfrac{\int_0^{b/2} c^2\,dy}{\int_0^{b/2} c\,dy}$, mean aerodynamic chord
S		Wing area
y		Length normal to plane-of-symmetry
Λ		Angle of sweepback
C_p	$=$	$(p_{loc} - p)/q$, pressure coefficient
p		Static pressure

LIST OF SYMBOLS—*continued*

q	Dynamic head of free stream
c_n	Section normal-force coefficient
c_m	Section pitching-moment coefficient, about section leading edge
$\bar{C}_n$	Overall normal-force coefficient
$\bar{C}_{m\,\bar{c}/4}$	Overall pitching-moment coefficient, about wing mean quarter-chord point
$\frac{c_n c}{c_{av}}$	Loading coefficient, at some particular value of $\bar{C}_n$
$\frac{c_n c}{\bar{C}_n c_{av}}$	Loading coefficient, general
ε	Angular rotation (deg) of line-of-flight chord line (' wash-out ')
$z_{c/4}$	Vertical displacement of quarter-chord point
α_r	Angle of incidence of root chord

---

1. *Introduction.*—When an unswept wing bends without twisting, there is no incidence change along the span, but bending of a swept wing produces components which appear in the line-of-flight as local changes of incidence and camber. Thus an upward bend causes a loss of incidence towards the tips. This feature reacts on the aeroelastic properties of a swept wing, particularly regarding aileron reversal, and calls for a close study of the relation of the bending and torsional stiffnesses of the wing. Longitudinal stability is also affected, since under normal acceleration in a turn the wings will bend, and the resulting loss of lift at the tips may produce a nose-up pitching moment tightening the turn or pull-out.

Another aspect of wing deformation is the possibility of incorporating some permanent incidence variation or the like in the construction of the wing, in order to alleviate some undesirable aerodynamic feature. For example, such a variation of incidence along the span might be used to produce an elliptic load distribution, or to delay tip stalling with its accompanying effect on the pitching moment.

The effects of wing deformation on the aerodynamic characteristics have only been investigated experimentally for a few special cases, even with unswept wings, and as the need for such results for swept wings is so much greater, it was felt that the development of a wing model which could be deformed into any desired mode warranted considerable effort. In addition to the value of the actual results for a specific plan-form, it was felt that experimental confirmation of some of the various theoretical methods available for the prediction of the characteristics of deformed wings would encourage the use of such methods for further analysis.

2. *The Technique of Deformable Models.*—2.1. *Perspex as a Model Material.*—The aerodynamic effects of wing deformation can be investigated by measuring the chordwise pressure distributions at a number of spanwise locations. The construction of a series of wooden pressure-distribution models, each with a particular mode of deformation, would be a difficult and laborious task, since at least six models would be required. Even with care in the matching of sections, it is questionable whether direct comparisons between the results from the individual models would be justified. Apart from these physical drawbacks, it would be difficult to predict what exact deformations are of interest, until at least three had been tested and some trends revealed.

It was therefore decided that the only practical proposition was the construction of a single model which could be deformed into any particular mode and ' set ' in that mode for pressure distribution testing. This suggested the use of a thermo-plastic material, and with this in view, the properties of Perspex were (*inter alia*) examined by the writer.

Perspex (polymethyl methacrylate) is a thermo-plastic material which, according to its temperature, behaves either as a hard brittle material with high tensile strength, or a rubber-like material with high deformability and weak mechanical strength. The temperature at melting is the ' first-order transition temperature ', and that of the change of behaviour is the ' second-order transition temperature ' ; the latter is not well-defined (Ref. 1). This ' second-order ' temperature depends on whether the Perspex had additional materials compounded with it. For unplasticised material it is about 100 deg C, dropping to 80 deg if plasticiser is added.

Under the appropriate temperature conditions the extremely long chain-like molecules of the Perspex, which are normally linked in a random fashion and coiled up, become partially straightened out under tensile stress. If cooled while this stress exists, the chains are ' frozen ', and the resulting deformation becomes permanent. Because the chains remain unbroken, however, the material has a high deformation recovery, the only requirement being the raising of the temperature back to the second-order transition value, when the chains will return to their original configuration.

Perspex may be easily cemented, a solvent of the material itself being used as a component of the cement. The surfaces to be joined are temporarily slightly softened when wetted with the cement, but after a time the cement is fully polymerized and the joint is virtually solid Perspex. The material is easily machined and worked by hand, and can be given a high surface finish.

In view of these properties, it was decided to construct a wing model from Perspex, the idea being to heat the model to the second-order transition temperature, deform it in its plastic state, and then cool it. This would ' freeze ' the deformation, enabling pressure distribution tests to be made for that particular deformation. It was hoped that this process could be repeated a number of times, and since the material has a ' memory ' in the sense explained above, the original undeformed model could always be regained by the simple process of heating, without then applying any mechanical stress, and allowing to cool.

2.2. *Geometric Details of the Wing.*—The wing plan-form selected was a semi-span model of the wing on the D.H.108 (*Swallow*) aircraft, having a 44-deg leading-edge sweepback, an aspect ratio of 4·3 and a taper ratio (tip chord/root chord) of 0·326 (Fig. 1). The aerofoil section was symmetrical, with a maximum thickness of 10 per cent chord at 40 per cent chord along wind. From leading edge to maximum thickness the section profile was elliptic, and from maximum thickness to the trailing edge, it was given by a quintic curve, with a 14-deg trailing-edge angle. (Section ordinates are given in Table 1.)

It was decided to distribute twenty-three pressure holes round the line-of-flight chords at eight spanwise locations. At each chord the holes were allocated as follows: one at the leading edge, one at the trailing edge, eleven over the upper surface and the remaining ten over the lower (Table 2).

2.3. *Construction of the Model.*—The Perspex selected for the construction of the model was unplasticized, since the second-order transition temperature of the material in that state is approximately 100 deg C. This temperature, it was thought, could be conveniently reached by boiling the model in a water tank. As the root chord of the plan-form was 14·85 in., giving a maximum thickness of just under $1\frac{1}{2}$ in., the Perspex was obtained in the form of $\frac{3}{4}$-in. thick flat sheet. The model was then made in the following stages.

Two blanks of the shape shown in Fig. 2 were cut from the sheet. These were slightly larger than the wing plan-form to allow for machining, and included a large portion of material which was to provide a root attachment for mounting in the wind tunnel and deforming frame. Channels

0·06-in. square were milled in the face of one of the blanks along the constant-percentage chord lines corresponding to the chordwise positions decided on for the pressure holes. In addition, two extra channels, one very close to the leading edge, and the other near the trailing edge, were provided to transmit pressures from the actual leading and trailing edges themselves.

The two blanks were clamped together and three locating holes were drilled through both blanks. Silver-steel pins were well-fitted into these holes. The positions of the alternate channels were carefully transferred to the non-milled blank by vertical scribing at the root and tip end faces, and the blanks were separated again.

Pressure holes 0·027-in. in diameter were then drilled at the appropriate spanwise locations to meet the appropriate chordwise channel.

The two blanks were then cemented together. The milled blank lay with the channels uppermost; lengths of copper wire were laid in the channels and a thick layer of cement was spread over the inner faces of the blanks. After a few minutes to allow for spreading, the upper blank was located on the pins, pressed firmly down on to the lower, and kept under pressure. The wires lying in the channels were kept in continuous agitation in order to keep the channels clear. After a few hours, the wires were withdrawn, as the cement appeared to be setting and no further flow was anticipated. The block was left in sunlight for a month, in order that the ultra-violet light should assist the polymerizing of the cemented joint; since it was obviously going to be extremely important that the joints between channels (which towards the tip were hardly $\frac{1}{16}$ in. wide) should not yield under deformation and allow pressure leakage from one channel to the next. Quarter-inch diameter Perspex tubes were cemented into the root ends of the channels to form connections for tubing.

The first stage in the profiling of the model was carried out on a vertical milling machine. The block was reduced in steps, both chordwise and spanwise (Fig. 3), the bottom corner of each step lying on the profile, plus a small allowance for finishing. The second stage was the hand-finishing to the correct profile with files and sandpaper, followed by the final polishing.

2.4. *The Deforming Frame.*—Since the heating medium for the model was to be boiling water, a frame was designed to serve two purposes; to support the model and water bath during boiling and to provide a rigid base for the deforming mechanisms and micrometers.

The main member of the frame (Figs. 4 and 5a) was a piece of 10-in. × 4-in. steel channel, which had planed surfaces and two parallel $\frac{1}{2}$-in. slots running the length of each flange. Brackets which held the model along its root line-of-flight chord were bolted to this channel, so that the wing leading edge was parallel to the base. Accurate locating distance pieces on the inner faces of these brackets ensured that the wing was always aligned properly when remounted on the frame after each test.

Side members which were slotted to carry the jacks and micrometers were made of 3-in. × 1-in. steel channel with machined surfaces. These members were mounted on the base so that when traversed along the flange slots they were aligned along the line-of-flight chords. Thus by moving the member to the appropriate spanwise position, and sliding a jack or micrometer along the chordwise slot in it, a force could be applied, or a measurement made, at any position on the wing.

The jacks were simple screwed rods in bushes, the ends of the rods being drilled to take different fittings, depending on the deformation requirements. In most cases, the deforming forces were applied through Tufnol contour boards, $\frac{1}{4}$-in. wide, which fitted the appropriate chord; slotted end fittings, free to rotate in the jack rods, then engaged the contour board.

The water bath, of capacity 6 gallons, was made of galvanized sheet steel and was held in position over the model by a small angle bracket at its bottom corner. Bunsen burners projected through holes in the base channel. This method of making a special tank with an opening cut off at the same angle as the sweep of the model, and then tilting the whole rig so that the line-of-flight chords were horizontal, was found to be the easiest solution of the problem of completely immersing the model without the complication of water-tight gaskets and seals, etc.

2.5. *The Technique for Producing Deformation.*—Before any deformation had been applied, the model as finished was carefully checked on a surface table.

The procedure for producing a deformation was as follows. With the undeformed wing locked in the frame, a contour board was fitted to the line-of-flight chord at which the deformation (for example, rotation about quarter-chord without vertical displacement of the quarter-chord line*) was to be applied. Two jacks were adjusted to line up with the diagonally opposite corners (*see* Fig. 5b) of the contour board. Micrometers were also adjusted across the other diagonal and the readings noted. The appropriate change in the readings of the micrometers to produce the desired deformation were then calculated and the new readings noted. A small allowance was found to be necessary to compensate for static recovery on cooling. This allowance varied with the mode of deformation and period of heating, but generally was of the order of 0·1 in.

Jacks and micrometers were then screwed back to give sufficient clearance for the water-tank, and the contour board removed. The tank was offered over the model and locked in place. It was then filled with water, so that the whole model was completely immersed, and the burners were lit. The water was kept boiling for three hours, and in some cases up to four hours.

At the end of this period, the water bath was removed as quickly as possible, commensurate with the awkwardness of handling six gallons of boiling water†, and the contour board was slipped on to the model. The micrometers were set to the readings decided upon, and the jacks were rapidly screwed up against the contour board. Very little effort was required to displace the contour board until it bore against the micrometer tips.

The model was then allowed to cool overnight, since any rapid thermal changes while the material was under high mechanical stress would produce thermal deformations in addition to those desired. When cooling was complete, the jacks were released and the model usually recovered very slightly.

It was found that even when Perspex becomes plastic to the extent indicated, it does not lose much of its surface hardness. There were thus no local deformations round the areas where the loads were applied. Consequently, there was no call for any elaborate means for spreading the load, such as pressure pads, etc. The quarter-inch wide contour board was found to be quite satisfactory in this respect.

If vertical displacement was also to be applied, the two jacks operated from the same side and pushed the model against the micrometers, which, in this case, had end fittings suitable as stops fitted at the opposite side (Fig. 5c). Photographs of a typical deformation of this type may be seen in Fig. 7.

To measure the deformation which had been applied, the model was removed from the rig and measured up on the surface table. The original steel chord templates used in making the model were used to check that no camber deformation had resulted from the main deformation, since the investigation was concerned only with the effects of local incidence change.

The low thermal conductivity of the model material allows a deformation mode to be built up in stages, working outwards from the root. This is simply done by filling the tank with water only to the level of the chord outboard of which it is desired to deform the model. The model remains quite cool, and therefore hard, right down to the water-line. Hence, when the deforming forces are applied to a contour board further outboard on the plastic region, the deformation inboard of the water-line remains unchanged. To prevent confusion with static deformation which can still occur in the cold portion of the model, it is better to lock the chord at the water-line before applying the deformation further outboard. The process could be repeated, using less water each time, until in the final stage only the tip chord is covered.

---

* The terms ' rotation ' and ' vertical displacement ' of a line-of-flight chord are used in this paper in preference to the more usual ' twist ' and ' bending ', since the latter terms are not explicit in themselves when applied to a swept-back wing, and can lead to confusion when the axes are not also specified.

† Experience soon showed that it was permissible to drain most of the water with the tank in position, using the tap in the bottom, and then lift off the almost empty tank. The model temperature did not alter during this procedure, presumably because of the steam rising from the water left in the tank.

The technique is extremely simple, and after one or two modes had been applied, it was possible to mount the model and have it boiling in about ten minutes. About the same time was required after the few hours boiling to remove the heating rig and apply the deformation. Rapid action in the latter operation is the key to success. It was noticeable how much stiffer the jacks became to turn if there had been even a few minutes delay in setting up the contour board, etc., with consequent cooling of the model. Various external heating devices were contemplated in the early development of the technique, but once the routine was established and successful deformations obtained, they were considered to be an unnecessary complication.

There does not appear to be any limit to the number of times a Perspex model can be heated and plastically deformed. Including deformations applied during development of the technique, the model described here has undergone about twelve cycles of heating, deformation and cooling, some of which involved very severe combined rotation and vertical displacement of inboard chords. There is to date no sign of any failure in the cemented surfaces, nor does the material appear to be losing its properties.

In the construction of future models it might be an advantage to use Perspex which contained some plasticizer, because of the resultant decrease in transition temperature, but there is some evidence to suggest that the plastic properties of such Perspex gradually decrease with repetition of the heating and cooling cycle.

On the whole, the Perspex of the model ' remembered ' its original form very well. After a particularly severe deformation, the model was heated for five hours, and allowed to cool without the application of load; it reverted to its original undeformed shape. The advantage claimed in this respect for Perspex as a model material would appear to be justified.

2.6. *Additional Advantages of Perspex.*—In addition to its ease of working and plastic properties, Perspex as a model material was found to have other advantages. Thus when it was decided to investigate the pressures very close to the model leading edge, it was comparatively simple to drill holes 0·025-in. diameter with a drill held in a pin-chuck and rotated with fingers only, at 0·01 and 0·025 of the chord, to meet the first channel inside the wing.

Again, when it was found desirable to have additional chordwise distributions at new spanwise locations, the necessary pressure holes could be drilled straight into the wing, the drill being directed visually to meet the appropriate channel, since the material is transparent.

Any damage to the model, for example, chipping of a tip, or indentation near a pressure hole, can be easily repaired by building up with cement. When set, this can be rubbed down and polished to match the original surface.

Its transparency lent itself very well to the use of ' silhouette ' techniques for the observation of wool tufts and liquid film studies, as described later.

3. *Pressure Distribution Tests.*—3.1. *Tests on the Undeformed Wing.*—A very exhaustive series of tests was carried out on the undeformed wing in an open-jet wind tunnel, at a Reynolds number of $0{\cdot}575 \times 10^6$, including a detailed study of the boundary-layer flow and the use of a liquid-film technique for the detection of separation ' bubbles ' and vortices near the leading edge (Ref. 2). These results provided a basis for comparison with the results from the deformed wing; they have for this reason been included in the figures in this report where relevant.

3.2. *The Range of Deformations Tested.*—In order to describe the mode of deformation, the setting of any particular line-of-flight chord on the wing, relative to the setting of the root chord, is expressed in terms of the vertical displacement of its quarter-chord point from the root chord plane, and the angular rotation of the chord line, measured from the root-chord datum.

The mode of deformation is therefore indicated in Fig. 6 by the spanwise distributions of the angular setting ε deg, and of the vertical displacement of the quarter-chord line, $z_{c/4}$, expressed as a ratio to the semi-span, $b/2$. Displacement is taken as positive upwards, and angular setting negative if there is a reduction in incidence (*see* Table 3).

Modes 1 and 2 (Fig. 6) were designed to represent continuously increasing ' wash-out ' of incidence towards the tip, without any vertical displacement. As can be seen, there was, in fact, a slight downward displacement near the tip, and the extreme tip section has a small ' wash-in ', due to an insert of Perspex there required for a repair.

Mode 3 was an attempt to simulate an isolated load on the wing at 0·7 semi-span, outboard of which there was no change in incidence. The vertical displacement in this case is not large and occurs mostly outboard of the load.

In order to determine the effects of vertical displacement on the pressure distributions, the same angular distribution along the span, but with considerably increased displacement, was aimed for. The success of this attempt may be judged from Mode 4, where the angular settings agree reasonably well with those of Mode 3 : but the quarter-chord line is now displaced 0·07 semi-span at the tip, compared with 0·015 for Mode 3.

Modes 5 and 6 may be regarded as extensions of the last two modes, in that the incidence along the span is first ' washed-out ' and then ' washed-in ' ; moreover, the degree of wash-in is increased to such an extent that the tip sections are actually at greater positive incidence than the root section. Thus the positive incidence of the tip section in Mode 5 is 1 deg, and in Mode 6 it is increased to 2·4 deg.

Mode 7 resulted from the application of an isolated load to the plastic wing well inboard and about $\frac{1}{3}c$ aft the leading edge. This produced a change of incidence starting much closer inboard, allied with a considerable vertical displacement at the tip.

A direct comparison of the angular setting distributions is included in Fig. 6b.

A physical idea of the deformation of the wing represented by the curves in Fig. 6 may be gained from Fig. 7, which shows photographs of Mode 7. The upper photograph is a view looking at the leading edge almost along the line-of-flight ; the rounding of the nose at the root chord indicates the slight obliquity of the view. In the lower photograph there does not appear to be much sweep angle because the view is actually along the quarter-chord line and not along the lateral axis of the wing. The smoothness of curvature of the leading and trailing edges shows up clearly, as does the nose-down setting of the tip chord. (The vertical block at the root of the wing is the root-fixing continuation of the model.)

3.3. *Presentation of Results.*—Chordwise pressure distributions were measured at each spanwise location in turn, over a range of root chord incidences from — 3 deg to 18 deg. For experimental convenience, the measurements for each deformation were made at the same values of root chord incidence, α_r, (Table 4). They were thus not directly comparable, since the overall lift at any particular root incidence varies with the deformation, and could not be related initially to α_r. In order to assess the effects of the deformations on the span loadings, these were made directly comparable by evaluating them at the same overall lifts. The procedure was as follows.

From the integrated chordwise pressure distributions the local normal-force coefficient, c_n, and pitching-moment coefficient, c_m, were obtained, and plotted against root incidence α_r for every mode. By further spanwise integration of the local coefficients, the overall normal-force coefficient, $\bar{C}_n$, and pitching-moment coefficient $\bar{C}_{m\,\bar{c}/4}$, (about the lateral axis through the mean quarter-chord) were obtained. From the curve of $\bar{C}_n$ against root incidence α_r, the root incidence corresponding to the same value of $\bar{C}_n$ as selected with the undeformed wing could be determined, and hence, from the curves of local coefficients c_n against α_r, the appropriate local coefficients could be found. The spanwise distribution of these could then be directly compared to the spanwise distribution previously obtained with the undeformed wing at the same selected value of $\bar{C}_n$ (Fig. 10 and Table 5).

4. *Discussion of Results.*—4.1. *Influence of Vertical Displacement (' Dihedral ') on Pressure Distributions.*—As already described, Modes 3 and 4 had almost identical incidence distributions, but the latter mode had considerable vertical displacement of the sections towards the tip (' dihedral '). Pressure measurements over a range of incidences for both deformations were made, and the distributions in each case, at low and high incidences, agreed almost perfectly.

This test, therefore, confirmed that the flow round any line-of-flight section of a swept-back wing is unaffected by the vertical displacement of the section relative to the root chord plane, at least up to a displacement of 0·07 semi-span at the tip.

4.2. *The Pressure Distributions for Various Modes.*—An important feature of the pressure distributions measured on the undeformed wing (Ref. 2) was the change in shape of the chordwise distributions at the tip as the incidence was increased above 12 deg. The peak suctions at the leading-edge collapse, and the tip-section distributions assume a ' triangular ' shape. With further increase in incidence, the distributions are almost flat, which is typical of the stall of thin aerofoils. At the same time, the ' triangular ' distribution moves further inboard, while peak suctions are maintained at the leading edge near the root (Fig. 8a)*.

A geometric wash-out of incidence towards the tip would be expected to delay the local onset of stalling, and such an improvement is obtained with the deformation of Mode 2, with nearly 6 deg of wash-out at the tip. Peak suctions are sustained over the tip region (Fig. 8b), but there is a dip in the suction about $\frac{3}{4}$ semi-span.

The effective incidence of the tip sections also depends upon the amount of upwash induced there by the sections further inboard, which are lifting strongly, as well as the geometric wash-out of the sections themselves. Thus a reduction in the lift of these inboard sections could help to reduce the effective incidence of the tip and delay the onset of stalling; to achieve this result the mid-semi-span sections, which in the undeformed state have the maximum lift, should have the maximum reduction of incidence, while the tip sections should, in fact, have their geometric incidence increased, in order to allow for the decreased lift-curve slope of these sections on a swept-back wing. Mode 3 represents such a deformation, with maximum wash-out at 0·7 semi-span.

The effect of this deformation on the pressure distributions as the incidence increases through the stalling range is striking (Fig. 8c). The section with maximum wash-out has a reduced suction over the upper surface, but inboard and outboard there are marked suction peaks. There is no sign of the collapse of the nose suction peaks towards the tip previously found with the undeformed model.

With Mode 6 (Fig. 8d) there is not such a pronounced dip in the suction ' carpet ', because there is less wash-out than in Mode 3. The wash-in of the tip appears to sustain the lift over the outer region, but some form of leading-edge stall at the tip is indicated by the highly localized suction peak, immediately downstream of which there is the typical ' flat ' distribution of the stalled aerofoil.

4.3. *Influence of Deformation on Spanwise Normal-force Coefficient Distribution.*—The effect of the deformations on the spanwise distribution of the sectional normal-force coefficient, c_n, at various values of the overall normal-force coefficient, $\bar{C}_n$, are shown in Figs. 9a to 9d (Table 5). These are discussed below for each mode in turn.

Mode 1.—The effect of ' wash-out ' is to reduce the value of c_n from the peak at 0·8 semi-span and to increase it inboard. There is a cross-over with the undeformed curve very near the tip at a $\bar{C}_n$ of 0·297 (Fig. 9a) which becomes much more marked at a $\bar{C}_n$ of 0·694 (Fig. 9c) when the undeformed wing has suffered tip stalling. At a $\bar{C}_n$ of 0·82 (Fig. 9d) the position of the peaks has reversed, as the outboard sections are benefiting from delayed stalling.

Mode 2.—Since this mode is similar in form to Mode 1, but with increased wash-out (5·67 deg at the tip compared to 3·84 deg with Mode 1) the values of c_n near the tip are more reduced, and correspondingly more lift is produced inboard. At a $\bar{C}_n$ of 0·82, the extreme tip has a small peak normal-force coefficient, but this may be due to the slight wash-in which existed there with this particular mode.

* Only the pressure distributions at the root incidence of 18 deg have been included in this paper. The same features can be seen at 12 deg and 15 deg.

Mode 3.—This mode has its maximum wash-out about 0·7 semi-span, with a slight reduction to the tip. At a $\bar{C}_n$ of 0·297 this produces an almost uniform c_n distribution over most of the span.

Mode 4.—This is maintained fairly well at $\bar{C}_n = 0{\cdot}583$, with a small localized dip near the tip. At a $\bar{C}_n$ of 0·694, the distribution is much improved over that of the undeformed wing, with the tip sections still unstalled. With further increase of $\bar{C}_n$ to 0·82, the benefits of this mode are very marked over the tip region, a mean section normal-force coefficient of about 0·7 being maintained.

Mode 5.—This mode differs from those above in having wash-in near the tip. The effect of this at $\bar{C}_n = 0{\cdot}297$ is to increase the local c_n at both root and tip and to reduce it between 0·6 and 0·8 semi-span.

At $\bar{C}_n = 0{\cdot}583$ this effect is more marked, but there is a localized dip about 0·9 semi-span. With increase to 0·694 the tip sections are lifting well, contrary to expectation with wash-in and even at 0·82 the distribution has its peak value outboard of that for the undeformed wing.

Mode 6.—The much greater wash-in towards the tip with this mode, compared to Mode 5, accentuates the re-distribution of c_n. At low incidence, there is a uniform, comparatively low c_n inboard, but over the tip region there is a marked peak.

At $\bar{C}_n = 0{\cdot}694$ the tip sections are attaining the highest c_n of all the modes, though their geometric angle of incidence is of the order of 17 to 18 deg. Even at $\bar{C}_n = 0{\cdot}82$ these sections are lifting strongly at a geometric incidence of about 20 deg.

Mode 7.—Because of its continuously increasing wash-out to the tip, the distributions for this mode resemble those of Modes 1 and 2.

4.4. *Spanwise Loadings at Zero Lift.*—The overall lift on the undeformed wing will be zero when all the sectional lifts are zero, and since the wing is of symmetrical section, the angle of incidence for no-lift will be 0 deg. At any given incidence measured from the no-lift angle, a spanwise loading distribution which is a function only of the incidence will exist.

When the wing has a spanwise variation of incidence, all the sectional lifts cannot be zero simultaneously, and zero overall lift will only occur at the incidence (measured for convenience at the root) at which the positive and negative lifts along the span are equal. This load distribution at the new angle of no-lift will be a function only of the particular variation of geometric incidence along the span, and is termed the ' basic ' loading.

If now the deformed wing is set at some incidence above the no-lift angle, but below the angle at which there is any local stalling, that is, within the linear range of the lift curves, then the total loading on the wing will be made up of the basic loading, and the ' additional ' loading due to the incidence change.

Experimentally, the additional loadings are those already measured on the undeformed wing (Ref. 2), and the total loadings on the deformed wing have been measured in these tests (section 4.3). The basic loading for each mode can therefore be found by subtracting the additional loading from the appropriate total loading measured at the same overall $\bar{C}_n$ (Fig. 10). It must be repeated that the loadings on the deformed wing may only be treated as the sum of the basic and additional loadings at sub-stalling incidences, since it has already been seen that the deformations have considerable effects on the stalling characteristics, and the additional loadings at these higher incidences do not then vary linearly with incidence: in consequence, basic and additional loading effects are then no longer additive.

4.5. *Spanwise Loadings at Sub-stalling Incidences.*—In order to compare the spanwise loadings of the various modes at incidences for which there is no stalling anywhere on the wing, they can be expressed in terms of the loading coefficient $c_n c/\bar{C}_n c_{av}$ for the selected value of $\bar{C}_n$ of 0·3. The loadings in this form are drawn in Fig. 12, with the loading for the undeformed wing included for comparison (Table 5).

All the deformations are effective in increasing the loading towards the root, and reducing it further outboard, to a greater or lesser degree. Thus Mode 2 at 0·2 semi-span has a local loading coefficient of almost 1·4 compared to 1·2 for the undeformed wing, but conversely at 0·8 semi-span the loading coefficient is only 0·4 compared to about 0·8.

Mode 3 produces almost as large a loading near the root, but the cross-over point of the curves is further inboard than with Mode 2, and hence the reduction of loading at any location outboard does not have to be so great. The distribution for this mode and $\bar{C}_n$ is the closest to elliptic loading obtained in the tests. The distributions with the modes having positive incidence at the tip have increased loading at root and tip and reduced loading between.

4.6. *Overall Normal-force and Pitching-moment Curves for the Various Modes.*—The variation of the overall normal-force coefficient, $\bar{C}_n$, with incidence, for the various modes is shown in Fig. 13 and tabulated in Table 4.

It will be seen that the slope, $d\bar{C}_n/d\alpha$, over the linear range, is unaffected by the deformation, being constant at 0·049 per degree for all the modes. There is some slight variation in the slope at the higher incidences, Mode 2 appearing linear over the whole range, and Mode 5 attaining the highest $\bar{C}_n$ measured for a root chord incidence, α_r, of 18 deg. In spite of the improved tip stalling characteristics resulting from the deformations already discussed, there is no appreciable improvement in the overall lift characteristics of the wing up to 18-deg incidence from any of the deformations.

The only experimental investigation of the effect of twist previously reported is that of Anderson (Ref. 3). With 8·5-deg wash-out at the tip of a 30-deg swept-back tapered wing, aspect ratio 6, he obtained an increase in $C_{L\,\max}$ from 1·4 at 20 deg with the untwisted wing to 1·5 at 25 deg with the twisted wing, the lift slope remaining constant. It would seem, therefore, that with the wing of this test, the influence of the various modes with regard to improvement in $C_{n\,\max}$ would only have appeared at incidences much higher than those tested.

The variation of the overall pitching-moment coefficient $\bar{C}_{m\,\bar{c}/4}$ with $\bar{C}_n$ is plotted in Fig. 14 for Modes 3, 6 and 7. If the axis of reference is assumed to be at the mean quarter-chord, then at low $\bar{C}_n$ Mode 7 has the maximum stability, but the break in stability arises at the lowest $\bar{C}_n$ With increase in $\bar{C}_n$ this mode remains more or less in neutral equilibrium.

Mode 3 has a curve of similar shape, but the break does not occur until a $\bar{C}_n$ of 0·5 is reached. It also has zero stability over the higher $\bar{C}_n$ range.

A considerable improvement in the stability characteristics is produced by the deformation of Mode 6. The static margin at low $\bar{C}_n$ is reduced below that of the undeformed wing, from about $0{\cdot}08\bar{c}$ to $0{\cdot}06\bar{c}$, but the stability continues to increase with $\bar{C}_n$ right up to a $\bar{C}_n$ of about 0·75.

The improvement in the stability characteristics of the wing with deformation arises from the sustained lift over the tip region, in contrast to the undeformed wing which has an early tip stall.

5. *The Effects of Deformation.*—There are two main aspects of the effects of deformation; one is concerned with the re-distribution of load at cruising incidence, mainly from the point of view of reducing induced drag, while the other arises at high incidence as a means of delaying tip stalling and retaining lateral control. The deformation itself may be either permanently constructed into the wing structure in order to produce a desired loading, or it may be brought about by loading under flight conditions.

5.1. *Low Incidence Loading.*—According to Munk's extension of Prandtl's induced-drag theory, elliptic span loading distribution produces minimum drag for a swept-back wing, as for an unswept wing. The distribution obtained for the undeformed wing, with its maximum value outboard, is therefore far from ideal in this respect.

It was noted earlier that for Mode 3 at a $\bar{C}_n$ of 0·3 the span loading was approaching the elliptic distribution (Fig. 11); this mode should therefore have had a reduced drag. Unfortunately, no balance drag measurements could be made to verify if this was so.

5.2. *Deformation and Tip Stalling.*—Modes 1, 2 and 7 with their continuously increasing wash-out from root to tip represent the type of deformation most likely to arise at high incidence from loading in flight. These deformations produce a slight gain in lift at the tips, which is contrary to their effect at low incidence. With the undeformed wing, the tip sections are well beyond their stalling incidence when the overall normal-force coefficient $\bar{C}_n$ is of the order of 0·7. Any decrease of effective incidence when the tip sections are in this condition should therefore be accompanied by an increased lift towards the tip.

This decrease of incidence can be brought about in two ways. Firstly, the reduction in geometric incidence of the tip sections brings them nearer to their incidence for $c_{n\,\max}$, and secondly, the reduction of incidence inboard of the unstalled sections results in less lift about 0·7 semi-span and consequently the upward induced velocity at the tip is also reduced. The addition of these two effects is enough to reduce the effective angle of incidence to almost the stalling value, and hence produce a c_n approaching $c_{n\,\max}$.

With Mode 3 the benefits at the tip are marked, even though the reduction in wash-out towards the tip would be expected to reduce the lift there. The main source of improvement here was thought to be the reduction in induced velocity, arising from the much more uniform lift inboard. This mode of deformation, with its improved tip-stalling behaviour and near-elliptic load distribution at a moderate overall lift coefficient, appears to warrant serious consideration as a permanent deformation to be built into a swept-back wing. Balance tests would be required to confirm this suggestion, and further investigations needed to establish the optimum location of the maximum wash-out and the actual amount of wash-out at any span location.

Modes 5 and 6 show how much the lift at the tip can be increased; the negative induction effects here must be very strong, especially in the latter mode, where the tip section is at 2·4-deg positive incidence to the root chord and yet is producing the largest local c_n of all the modes, with a geometric incidence of over 20 deg. This type of deformation, with its inferior load distribution at low incidence, cannot be considered as a permanent deformation, but the unstalled flow over the tip region at large $\bar{C}_n$ (Fig. 9d), which would presumably help lateral control on landing, is a prize worth striving for, and might be achieved by some form of flap.

5.3. *Liquid-Film Study on a Deformed Wing.*—The flow in the boundary layer of the undeformed wing had been studied with the aid of a liquid film technique (Ref. 2); this consisted of spraying the wing with a suspension of lamp-black in paraffin with the wind off, then turning the wind on rapidly. The lamp-black pattern then indicated the general flow of the boundary layer.

Briefly, the most important features found with the undeformed wing were:

(*a*) the formation of a separation bubble under the separated layer near the leading edge at incidences from 6 deg to 9 deg, extending from root to tip,

(*b*) an abrupt change in direction of the flow of liquid along the leading edge about mid-semi-span at about 9 deg, so that it flowed chordwise across the wing, reaching the trailing edge,

(*c*) the growth of a rotating accumulation of fluid at the leading edge at the tip about 12 deg. This moved inboard with increase of incidence, until at 18 deg it was only about $\frac{1}{3}$ semi-span from the root chord.

The lamp-black technique was unfortunately only developed after the programme of tests on the deformation modes was completed. In order to obtain some general idea of the influence of deformation on the unusual boundary-layer flow detected on the undeformed wing, a typical deformation (roughly between Modes 3 and 6) was produced in the model and lamp-black patterns obtained.

At 12 deg the accumulation of fluid parallel and close to the leading edge bifurcates about mid-semi-span, some of the flow going in a broad band across the wing to the trailing edge, and the remainder proceeding along the leading edge almost to the tip. About 0·9 semi-span, this also turns along the line-of-flight, and the tip region is covered with a broad band flowing aft.

With increase to 15 deg (Fig. 15) the pattern resembles more closely those obtained on the undeformed wing at lower incidence. A rotating accumulation of fluid appears at about 0·8 semi-span on the leading edge, and the liquid flowing parallel to the leading edge at the root has turned aft about 0·4 semi-span. The new feature due to the deformation is a second rotating accumulation at the leading edge about mid-semi-span which sends out streamers of fluid both across the wing and along the leading edge to the outer accumulation.

At 18 deg there is the same outward flow along the trailing edge, as with the undeformed wing, followed by a sharp curving-round with flow inwards along the leading edge to the rotating mass at about 0·7 semi-span.

The new accumulation already noted on the leading edge about mid-semi-span at 15 deg is now much larger. Fluid flows in a spanwise direction, skirting past this accumulation, and proceeds outwards to feed the outer one. This flow along the boundary of the inner accumulation can be seen as a slightly thicker dark band surrounding the core.

The interpretation of these liquid-film patterns is still difficult, since it has not yet been established whether the liquid film moves mainly under the influence of the shear stress of the air in the boundary layer, or whether it is more powerfully influenced by the pressure gradients existing on the wing surface. A comparison of the pattern in Fig. 15 at 18 deg with the pressure contours for Mode 3 in Fig. 8c indicates that the two rotating fluid accumulations are located at the two suction peaks located on either side of the section with maximum wash-out.

6. *Theoretical Prediction of Wing Characteristics.*—The characteristics of the undeformed wing have already been calculated using the Weissinger, Diederich and Stanton-Jones methods (Ref. 2). The Weissinger method is very conveniently applied for the prediction of the loadings on the deformed wing, especially if the aerodynamic influence coefficients of the wing are already known from the undeformed case (Ref. 5). The Diederich method, which is a simple semi-empirical one, can also be applied to a deformed wing (Ref. 6). An outline of the methods is given in Appendix I.

Both methods were used to predict the basic loading on the deformed wing for all modes. This basic loading was then added to the additional loading already calculated by these methods for the undeformed wing (Ref. 2). The gross loadings so obtained are shown in Fig. 16.

6.1. *Span Loading Distribution.*—It is immediately obvious from Fig. 16 that the points at the four spanwise locations given by the Weissinger solution are insufficient to cope with any fairly abrupt changes in angular setting along the span (Table 6). Thus, for example, the loading of Mode 2, which has a smooth wash-out to the tip, is predicted quite accurately, except for the overload at the centre, whereas that for Mode 6, which has both wash-out and wash-in, shows poor agreement if the theoretical points are joined with smooth curves.

The actual local values for most of the modes are in good agreement, which suggests that increasing the number of spanwise locations in the theory would probably improve the shape of overall distribution. The ability of the theory to produce such agreement at isolated points is really quite good when the powerful induction effects arising from the variation in effective incidence along the wing are considered.

An important aspect of any theoretical method is its ability to predict the distribution of angular setting required to produce a desired loading, for example, an elliptic distribution. This would be the inverse problem of the result obtained for Mode 3, where the distribution was first obtained experimentally and the Weissinger theory applied to the particular deformation.

From Fig. 16 it appears that the Weissinger method applied to this type of deformation gives a very good estimation of the loading, and so could be used with any given plan-form for the prediction of the deformation necessary to produce an elliptic distribution.

DeYoung and Harper (Ref. 4) compare the basic span loading predicted by the Weissinger theory with that measured on a wing with 60·8 deg quarter-chord sweepback, and with wash-out increasing continuously to 19 deg at the tip. They find agreement of the same order as that obtained here with similar forms of deformation, for example, Mode 2.

The Diederich method, which for the basic loading is simply the Schrenk approach, gives remarkably good agreement, especially in the shape of the distribution curves. For the curves plotted, a value for the overall wing lift-curve slope of 0·050 per degree was used; this was the experimentally determined value. The drawback to this method, from the point of view of using it to predict the characteristics of an untested plan-form, is that the accuracy is dependent on the assumption of the overall lift-curve slope. If, however, an undeformed wing has been balance tested, so that $dC_L/d\alpha$ is known, the Diederich method will give a rapid prediction of the span loading and the effect of any particular wing deformation on it.

6.2. *Pitching Moment at Zero Lift.*—The basic loading gives rise to a pitching moment at zero overall lift. This pitching moment, expressed as a coefficient, $C_{m\,0}$, can be calculated by the Weissinger method.

As the pitching-moment curves from the experimental results were only obtained for Modes 3, 6 and 7 (Fig. 14), owing to the computing effort required, the coefficients for the same three modes are the only ones calculated theoretically. The results are as follows:

$\bar{C}_{m\,0}$

	Mode 3	Mode 6	Mode 7
Measured ..	0·018	0	0·017
Weissinger ..	0·023	0·0004	0·0166

The Weissinger method thus predicts the basic pitching moment quite accurately, even for modes where the predicted distribution did not agree too well because of wash-out and wash-in. This presumably is because, as already mentioned, the isolated loads are reasonably accurate, and when integrated to give pitching moments, the discrepancy between the shape of the distribution curves becomes less significant.

DeYoung and Harper (Ref. 4) applied the Weissinger method to Anderson's tested wing (Ref. 3), which had 30 deg sweepback and 8·5 deg wash-out at the tip. The force tests gave a $\bar{C}_{m\,0}$ of 0·05, which is the same as that predicted from theory.

6.3. *Root Angle of Incidence for No Lift.*—Both the Weissinger and Diederich methods predict the root angle of incidence for zero lift. The experimental values cannot be obtained very accurately, since they must be read off the intersection of the normal force curve and the axis. The values are as follows:

$\alpha_{r\,0}$ degrees

Modes	1	2	3	5	6	7
Measured ..	0·7	1·5	2·2	0·10	0·5	1·4
Weissinger ..	0·53	1·08	1·95	0·76	0·85	1·31
Diederich ..	0·57	1·0	2·0	0·51	0·78	1·3

The predictions here are reasonably good, except for Modes 2 and 5 where both theoretical values agree, but differ from the measured value. For Anderson's wing DeYoung and Harper predicted a no-lift angle of 3·3 deg, compared to the measured value of 2·6 deg.

The agreement between the Weissinger result, in which induction effects are included, and the Diederich result, which is simply the mean geometric incidence of the deformed wing, is remarkable.

7. *Conclusions.*—7.1. A simple technique for the construction of wind-tunnel models which can be easily deformed and set into any desired mode of deformation has been developed. The model is made of Perspex which when heated to 100 deg C. becomes plastic; in this state the deformation can be applied through contour boards fitted to the wing. On cooling, the wing is 'frozen' into its deformed shape, and it can then be tested in the wind tunnel in this state.

7.2. Vertical displacement of any line-of-flight chord ('dihedral') up to 0·07 semi-span at the tip did not affect the pressure distribution round it. The pressure distribution is only affected by the spanwise distribution of incidence along the wing.

Any decrease of incidence ('wash-out') towards the tip is effective in reducing the loading on the wing outboard, and increasing it inboard towards the root, at low overall lift coefficients. In order to produce a near elliptic loading at a design C_L it appears necessary to have maximum wash-out at about 0·7 semi-span and to reduce it outboard to the tip.

This type of deformation also improved the stalling characteristics of the wing at high incidence, with the tip region sustaining much more lift. The maximum improvement in tip stalling was produced by having wash-out extending from the root to a maximum at about mid-semi-span, with wash-in towards the tip. This deformation gives a poor loading distribution at low incidence, however, and would only be worthwhile if it could be effectively produced by (say) deflection of flaps when required at high incidence.

Since all the deformations tested increased the lift at the tip region and delayed the stall there, the characteristic change of slope in the pitching-moment curve of the undeformed wing, arising from tip stall, was eliminated.

7.3. Liquid-film studies of the boundary-layer behaviour showed rotating accumulations of fluid inboard and outboard of the section with maximum wash-out. Comparison with pressure distributions confirms that there exist suction peaks at these localized regions of accumulated fluid; this suggests that some form of 'standing' vortex is induced in the flow over the wing, and the beneficial effect of mid-semi-span wash-out allied with wash-in to the tip on tip stalling is associated in some way with this new vortex system.

7.4. The Weissinger method for predicting the characteristics of deformed sweptback wings gave reasonably accurate results at low incidence. Very little computing effort was required to predict the effects of deformation once the influence coefficients of the wing geometry had been determined.

REFERENCES

No.	Author	Title, etc.
1	H. Warburton Hall and E. W. Russell	Polymethyl methacrylate plastics: Crazing, thermal and mechanical properties. R. & M. 2764. October, 1949.
2	Joseph Black	Pressure distribution and boundary-layer investigations on a 44-deg swept-back tapered wing. Part I. Three-dimensional tests on the wing. Part II. Two-dimensional pressure distribution tests on a 10 per cent thick symmetrical aerofoil section. C.P.137. January, 1953.
3	R. Anderson	Determination of the characteristics of tapered wings. N.A.C.A. Report No. 572. 1936.
4	J. DeYoung and C. W. Harper ..	Theoretical symmetric span loading at subsonic speeds for wings having arbitrary planform. N.A.C.A. Report No. 921. 1948.
5	V. I. Stevens	Theoretical basic span loading characteristics of wings with arbitrary sweep, aspect ratio and taper ratio. N.A.C.A. Tech. Note No. 1772. December, 1948.
6	F. W. Diederich..	A simple approximate method for obtaining spanwise lift distributions over swept wings. N.A.C.A. RM L7107. May, 1948.

APPENDIX I

*The Weissinger Method for the Prediction of Loading due to Twist on a Swept-back Wing**

1.1. The representation of the wing for the Weissinger method is shown in Fig. 17. The gross circulation, representing both additional and basic loading, is concentrated along the quarter-chord line, and the downwash at any point on the surface is therefore produced by this swept lifting-line and its system of trailing vortices.

For the additional loading, that is, for the untwisted wing, the method may be summarized as the solution of four simultaneous equations of the form

$$\alpha_\nu = \sum_{n=1}^{4} a_{\nu n} G_n \quad .. \quad .. \quad .. \quad .. \quad .. \quad .. \quad .. \quad (1)$$

where α_ν is the slope of the camber-line at the $\frac{3}{4}c$ point for the spanwise station ν, $a_{\nu n}$ are the influence coefficients dependent on wing geometry, and G_n are the dimensionless circulations.

For the additional loading, the angle of incidence is constant along the span and equation (1) becomes

$$1 = \sum_{n=1}^{4} a_{\nu n} \frac{G_n}{\alpha_\nu} . \quad .. \quad .. \quad .. \quad .. \quad .. \quad .. \quad (2)$$

In the case of basic loading, however, α_ν varies across the span, and the equations must be used in the form of equation (1). For a particular deformation, the variation in α_ν across the span will be known, but the actual value of α_ν at each station which will satisfy the unique condition of zero overall lift on the wing is unknown. There are thus only four simultaneous equations with eight unknowns, namely, the four α_ν and four G_n.

* This application of Weissinger's method is discussed in ' Theoretical Basic Span Loading Characteristics of Wings with Arbitrary Sweep, Aspect Ratio, and Taper Ratio '. V. I. Stevens, N.A.C.A. Tech. Note 1772. December, 1948.

If the angle of incidence of the root mean camber line at $\frac{3}{4}c$ at zero overall lift ($C_L = 0$), is designated $(\alpha_r)_0$, then

$$(\alpha_v)_0 = (\alpha_r)_0 + \varepsilon_v \,, \qquad \ldots \qquad (3)$$

where $(\alpha_v)_0$ is the section incidence at $C_L = 0$, and ε_v is the section twist relative to the root chord (*see* Fig. 17). The use of equation (3) reduces the unknowns to five, that is, $(\alpha_r)_0$ and G_n.

The equation for the lift coefficient C_L is given by

$$C_L = \frac{\pi \text{ A.R.}}{m+1}\left(\frac{G_m + 1}{2} + 2\sum_{n=1}^{\frac{m-1}{2}} G_n \sin \phi_n\right)$$

or

$$C_L = \frac{\pi \text{ A.R.}}{8}\left(G_4 + 2\sum_{n=1}^{3} G_n \sin \phi_n\right). \qquad \ldots \qquad (4)$$

This equation provides the fifth equation necessary to determine the five unknowns, since $C_L = 0$ and $\phi_n = n\pi/8$, leaving only G_n. The final set of simultaneous equations for finding the loading G_n and the root incidence for no-lift are

$$\left.\begin{aligned}
\varepsilon_1 &= -(\alpha_r)_0 + a_{11}G_1 + a_{12}G_2 + a_{13}G_3 + a_{14}G_4 \\
\varepsilon_2 &= -(\alpha_r)_0 + a_{21}G_1 + a_{22}G_2 + a_{23}G_3 + a_{24}G_4 \\
\varepsilon_3 &= -(\alpha_r)_0 + a_{31}G_1 + a_{32}G_2 + a_{33}G_3 + a_{34}G_4 \\
\text{(Root chord)} \quad 0 &= -(\alpha_r)_0 + a_{41}G_1 + a_{42}G_2 + a_{43}G_3 + a_{44}G_4 \\
(C_L = 0) \quad 0 &= 0{\cdot}7651G_1 + 1{\cdot}414G_2 + 1{\cdot}848G_3 + G_4
\end{aligned}\right\} \ldots \qquad (5)$$

Solution of this set of equations gives $(\alpha_r)_0$ and the loads at span stations, $\eta = 0{\cdot}924$, $0{\cdot}707$, $0{\cdot}383$ and 0.

The inverse problem of determining the twist necessary to produce a given basic load distribution is only a matter of inserting the appropriate values of G_n and solving for ε_v.

The values of a_{mn} are the coefficients of G_n/α which are functions of the wing geometry. Hence, while some labour is required to compute them, they only need to be determined once for any particular plan-form*. Variations in twist and camber of this plan-form are then easily investigated, since each deformation mode only calls for the solution of a set of five simultaneous equations.

The actual loading in terms of $c_{l_b}c/c_{\text{av}}$ is given by

$$\left(\frac{c_{l_b}c}{c_{\text{av}}}\right)_n = 2 \text{ A.R. } G_n \,. \qquad \ldots \qquad (6)$$

The pitching-moment coefficient, $C_{m_b} = M_b/qS\bar{c}$ is given by

$$C_{m_b} = -\frac{b/2}{2}\tan \Lambda \,(0{\cdot}1384k_{1_b} + 0{\cdot}1975k_{2_b} + 0{\cdot}1351k_{3_b} + 0{\cdot}0159k_{4_b}) \ldots \qquad (7)$$

As this pitching moment arises from a loading couple, it is independent of the location of a reference point, unlike the additional moment which is usually taken about the mean quarter-chord point.

As there were no experimental data available on basic span loading, Stevens used the results given by Falkner's method as a criterion for the accuracy of Weissinger's basic load results. This is justified on the grounds that the Falkner method is based on a lifting surface, and is consequently inherently more accurate.

* Stevens has tabulated these coefficients for aspect ratios 1·5, 2·5, 3·5, 4·5, 6·0, 8·0 and 10, sweep -45, -30, 0, 30, 45, 60 and 75 deg, and taper ratio 0, 0·25, 0·5, 1·0 and 1·5. For a rapid estimation of a plan-form not given in the Tables, it is possible to interpolate the loadings of the two bracketing plan-forms.

1.2. *Solution for the Deformed Wing.*—To set up the five simultaneous equations required, the incidence at each of the control locations, ε_r, is inserted in equation (5). Thus, as an example, the set of equations for Mode 7 is as follows :

$$(1) \qquad -\frac{3\cdot4}{57\cdot3} = -(\alpha_r)_0 + 11\cdot174G_1 - 3\cdot7305G_2 + 0\cdot1503G_3 - 0\cdot3098G_4$$

$$(2) \qquad -\frac{3\cdot03}{57\cdot3} = -(\alpha_r)_0 - 1\cdot4692G_1 + 6\cdot4601G_2 - 2\cdot4375G_3 + 0\cdot1207G_4$$

$$(3) \qquad -\frac{0\cdot95}{57\cdot3} = -(\alpha_r)_0 + 0\cdot1004G_1 - 1\cdot3071G_2 + 5\cdot0509G_3 - 1\cdot6985G_4$$

$$(4) \qquad 0 = -(\alpha_r)_0 - 0\cdot1474G_1 + 0\cdot2414G_2 - 2\cdot5101G_3 + 4\cdot4676G_4$$

$$(5) \qquad 0 = 0\cdot765G_1 + 1\cdot414G_2 + 1\cdot848G_3 + G_4 .$$

The matrix solution is set up below:

G_1	G_2	G_3	G_4	$(\alpha_r)_0$	Constant	Check Column $= \Sigma$ cols.
11·174	−3·7305	0·1503	−0·3098	−1·0	−0·05934	6·2247
− 1·4692	6·4601	−2·4375	0·1207	−1·0	−0·05288	1·6212
0·1004	−1·3071	5·0509	−1·6985	−1·0	−0·01658	1·1291
− 0·1474	0·2414	−2·5101	4·4676	−1·0	0	1·0515
0·765	1·414	1·848	1·0	0	0	5·0270
11·174	−0·3339	0·01345	−0·02773	−0·08949	−0·00531	0·5570
− 1·4692	5·9695	−0·4050	0·01339	−0·1895	−0·01017	0·4087
0·1004	−1·2736	4·5337	−0·3703	−0·2718	−0·0064	0·3515
− 0·1474	0·1992	−2·4303	3·5610	−0·4598	−0·00402	0·5354
0·765	1·6694	2·5138	1·9297	1·9553	0·02295	1·0238

Hence

$$\text{Root incidence for no-lift} = (\alpha_r)_0 = 0\cdot229 \text{ radians}$$
$$= \underline{1\cdot315 \text{ degrees}}$$

Span Loading

The loadings at the four spanwise locations are thus

$$G_4 = -0\cdot004016 + 0\cdot4598(\alpha_r)_0 = 0\cdot006536$$
$$G_3 = -0\cdot006396 + 0\cdot2718(\alpha_r)_0 + 0\cdot3703G_4 = 0\cdot002262$$
$$G_2 = -0\cdot01017 + 0\cdot1895(\alpha_r)_0 - 0\cdot01339G_4 + 0\cdot405G_3 = -0\cdot004992$$
$$G_1 = -0\cdot00531 + 0\cdot08949(\alpha_r)_0 + 0\cdot02773G_4 - 0\cdot01345G_3 + 0\cdot3339G_2 = -0\cdot004772 .$$

From equation (6) the actual loadings in terms of the coefficient $c_l c/c_{av}$ are as follows:

n	$\left(\frac{c_l c}{c_{av}}\right)_0$
1	−0·04104
2	−0·04293
3	0·01945
4	0·05621

Basic Pitching-Moment Coefficient

Substitution in equation (7) gives

$$C_{m0} = -\left(\frac{b/2}{10{\cdot}7} \times 0{\cdot}8391\right)(-0{\cdot}01064)$$

therefore

$$C_{m0} = 0{\cdot}0166$$

TABLE 1

Aerofoil Section Ordinates

Distance from leading edge (per cent c)	Semi-height of section (per cent c)
1·0	1·10
2·5	1·73
5·0	2·42
7·5	2·89
10·0	3·30
15	3·90
20	4·32
25	4·63
30	4·84
35	4·97
40	5·00
50	4·83
60	4·31
70	3·48
80	2·42
90	1·22
100	0

TABLE 2

Position of Pressure Holes

	Hole No.	x (per cent c)
Upper Surface	1	L.E.
	2	5
	3	10
	4	20
	5	30
	6	40
	7	50
	8	60
	9	70
	10	80
	11	87·5
	12	95
	13	T.E.
Lower Surface	14	7·5
	15	15·0
	16	25
	17	35
	18	45
	19	55
	20	65
	21	75
	22	85
	23	92·5

TABLE 3

Vertical Displacements and Angular Settings along the Span for the Various Modes

Span location								Deformation
$\frac{y}{b/2}$	0·02	0·2	0·44	0·56	0·68	0·83	0·93	0·97	
$\frac{z_{c/4}}{b/2}$	0	0	−0·0003	−0·0008	−0·0011	−0·0030	−0·0023	−0·0021	Mode 1
ε (deg)	0	0	−0·05	−0·37	−0·97	−2·47	−3·82	−3·72	
$\frac{z_{c/4}}{b/2}$	0	0	0·0009	−0·0005	−0·00067	−0·0027	−0·0037	−0·0025	2
ε (deg)	0	0	−0·47	−0·975	−2·275	−4·525	−5·62	−5·67	
$\frac{z_{c/4}}{b/2}$	0	0·00075	0·0021	0·0017	0·0062	0·0123	0·0138	0·0145	3
ε (deg)	0	−0·275	−2·22	−4·24	−4·53	−4·21	−4·075	−4·04	
$\frac{z_{c/4}}{b/2}$	0	0·0009	0·0115	0·0224	0·0365	0·0520	0·0608	0·0644	4
ε (deg)	0	−0·33	−3·142	−4·38	−4·27	−4·16	−4·22	−3·48	
$\frac{z_{c/4}}{b/2}$	0	0·0003	0·0066	0·0110	0·0210	0·0280	0·0310	0·0310	5
ε (deg)	0	−0·12	−1·46	−1·008	−0·66	−0·28	0·68	0·9	
$\frac{z_{c/4}}{b/2}$	0	0·0005	0·0072	0·0145	0·0250	0·0371	0·0407	0·0406	6
ε (deg)	0	−0·183	−2·21	−3·07	−2·23	1·15	2·23	2·4	
$\frac{z_{c/4}}{b/2}$	0	0	0·005	0·0119	0·0234	0·0415	0·0527	0·0580	7
ε (deg)	0	−0·067	−1·2	−2·1	−2·78	−3·59	−3·81	−3·83	

TABLE 4

Variation of $\bar{C}_n$ with α for the Various Modes

α_r (deg)	$\bar{C}_n$						
	Undeformed	1	2	3	5	6	7
− 3	—	−0·19	−0·22	−0·26	−0·167	−0·188	−0·204
0	0	−0·035	−0·081	−0·117	−0·013	−0·048	−0·064
6	0·297	0·274	0·238	0·23	0·307	0·292	0·244
9	0·446	0·422	0·378	0·355	0·466	—	0·375
12	0·583	0·575	0·547	0·501	0·616	0·587	0·530
15	0·694	0·694	0·679	0·642	0·743	0·701	0·651
18	0·826	0·805	0·844	0·811	0·852	0·804	0·815

TABLE 5

Spanwise Distributions of c_n and $\frac{c_n c}{\bar{C}_n c_{av}}$ for the Various Modes

$\bar{C}_n$	Span location $\frac{y}{b/2}$								Mode
	0·02	0·2	0·44	0·56	0·68	0·83	0·93	0·97	
0·297 (6°)	0·223	0·276	0·333	0·338	0·386	0·377	0·296	0·24	Undef.
	—	0·280	0·32	0·34	0·32	0·30	0·23	0·23	1
	0·27	0·32	0·35	0·33	0·33	0·4	0·17	0·14	2
	—	0·32	0·31	0·30	0·33	0·32	0·25	0·22	3
	—	0·29	0·34	—	0·36	0·37	0·29	0·24	5
	—	0·27	0·27	0·31	0·34	0·42	0·38	—	6
	0·26	0·30	0·32	0·33	0·34	0·31	0·22	0·14	7
0·583 (12°)	0·448	0·56	0·648	0·708	0·704	0·674	0·634	0·517	Undef.
	—	0·55	0·65	0·67	0·66	0·64	0·50	0·46	1
	0·49	0·59	0·67	0·65	0·69	0·60	0·44	0·38	2
	—	0·60	0·63	0·64	0·64	0·65	0·55	0·58	3
	—	0·55	0·62	—	0·71	0·73	0·60	0·70	5
	—	0·56	0·60	0·62	0·71	0·76	0·86	—	6
	0·48	0·56	0·665	0·67	0·72	0·56	0·52	0·41	7
0·694 (15°)	0·552	0·675	0·818	0·851	0·920	0·654	0·440	0·321	Undef.
	—	0·69	0·81	0·82	0·84	0·66	0·63	0·58	1
	0·58	0·71	0·81	0·78	0·78	0·65	0·46	0·49	2
	—	0·74	0·80	0·80	0·80	0·79	0·66	0·71	3
	—	0·66	0·74	—	0·85	0·90	0·71	0·56	5
	—	0·66	0·74	0·76	0·80	0·96	0·91	—	6
	0·60	0·70	0·83	0·84	0·90	0·63	0·63	0·34	7
0·82 (18°)	0·684	0·864	1·112	1·074	0·888	0·542	0·394	0·257	Undef.
	—	0·83	0·97	1·08	0·82	0·59	0·49	0·48	1
	0·67	0·88	0·94	1·0	0·81	0·59	0·45	0·52	2
	—	0·82	0·92	0·93	0·88	0·71	0·69	0·70	3
	—	0·82	0·91	—	1·02	0·83	0·54	0·37	5
	—	0·78	0·87	0·97	1·01	0·97	0·80	—	6
	0·68	0·83	0·96	1·03	0·92	0·67	0·43	0·25	7
$\frac{c_n c}{\bar{C}_n c_{av}}$ $\bar{C}_n = 0·297$	1·09	1·19	1·155	1·03	1·02	0·817	0·528	0·392	Undef.
	—	1·21	1·11	1·04	0·842	0·636	0·41	0·376	1
	1·32	1·38	1·215	1·01	0·87	0·51	0·304	0·229	2
	—	1·38	1·075	0·916	0·87	0·679	0·465	0·36	3
	—	1·24	1·16	—	0·935	0·775	0·519	0·40	5
	—	1·205	0·966	0·949	0·942	0·901	0·688	—	6
	1·27	1·29	1·11	1·01	0·895	0·656	0·392	0·229	7

TABLE 6

Spanwise Distributions of $\frac{c_l c}{\bar{C}_L c_{av}}$

Predicted by Weissinger Theory for the Various Modes

$\frac{y}{b/2}$				State of wing
0	0·383	0·707	0·924	
1·198	1·151	0·944	0·566	Undeformed
1·296	1·222	0·874	0·443	1
1·379	1·258	0·809	0·320	2
1·472	1·234	0·730	0·404	3
1·252	1·091	0·949	0·629	5
1·278	1·108	0·879	0·685	6
1·387	1·216	0·799	0·428	7

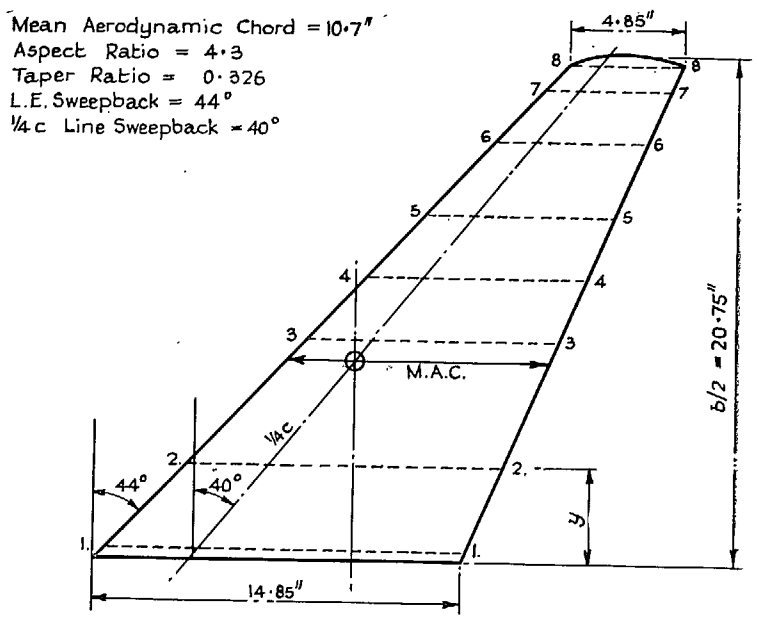

Chord	1	2	3	4	5	6	7	8
Span Position y/ b/2	0·02	0·2	0·44	0·56	0·68	0·83	0·93	0·97

Aerofoil Section: 10% thick at 40% c

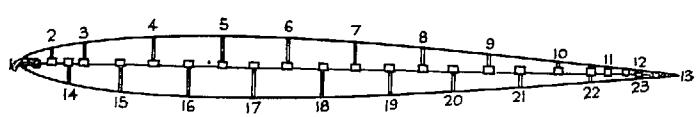

FIG. 1. Details of wing and pressure holes.

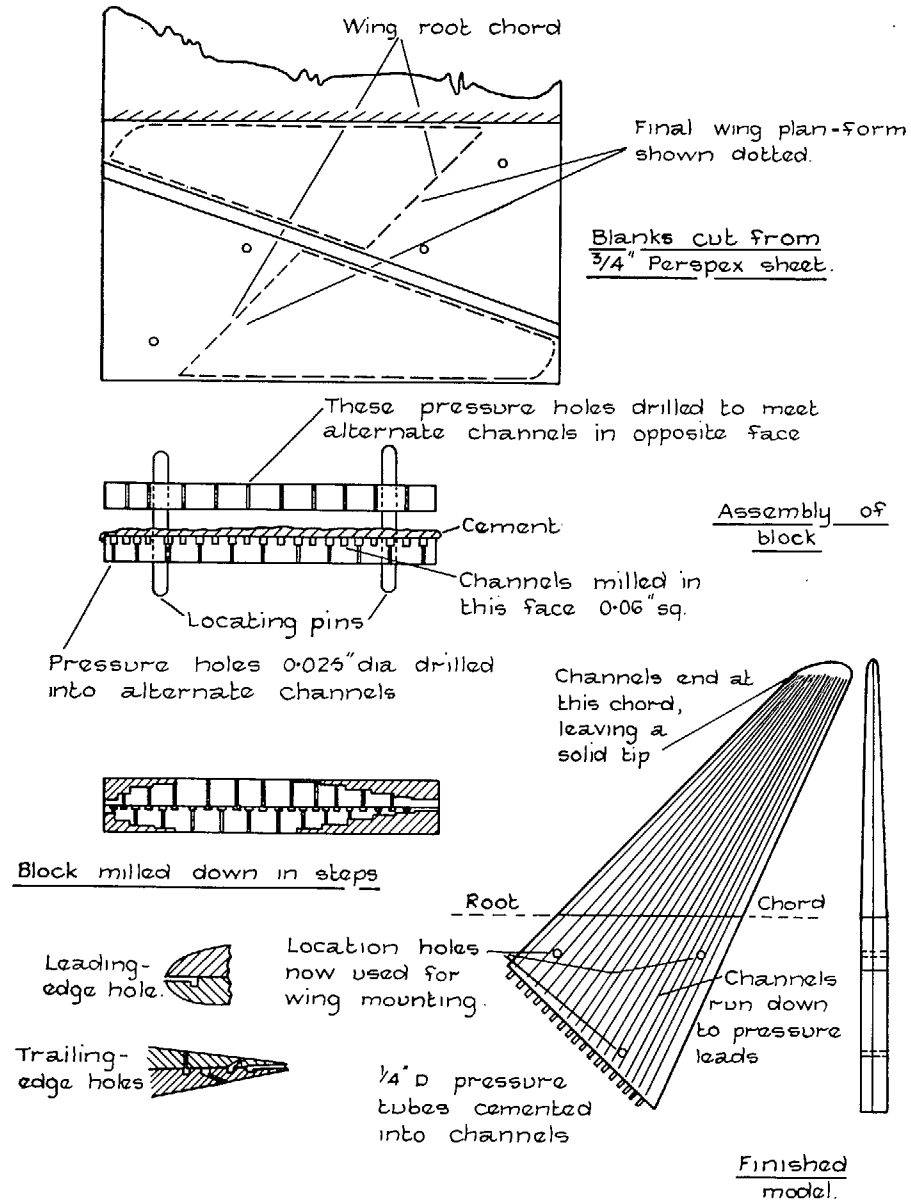

FIG. 2. Details of model construction.

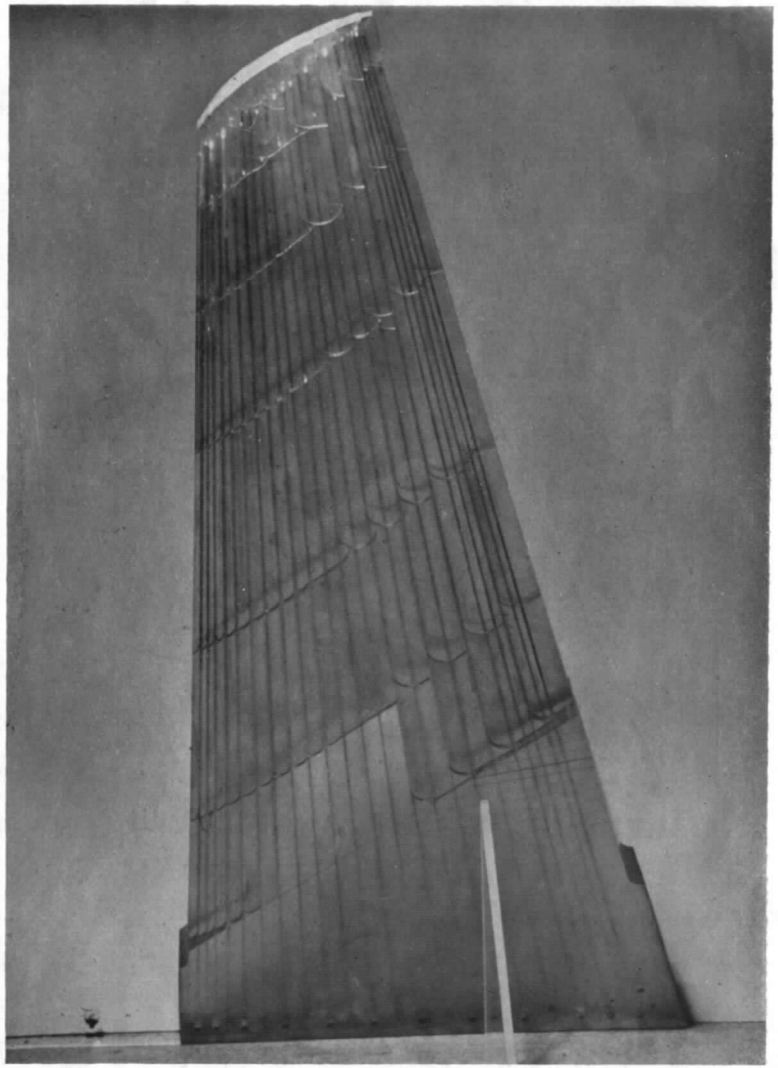

FIG. 3. The block step-milled, ready for profiling.

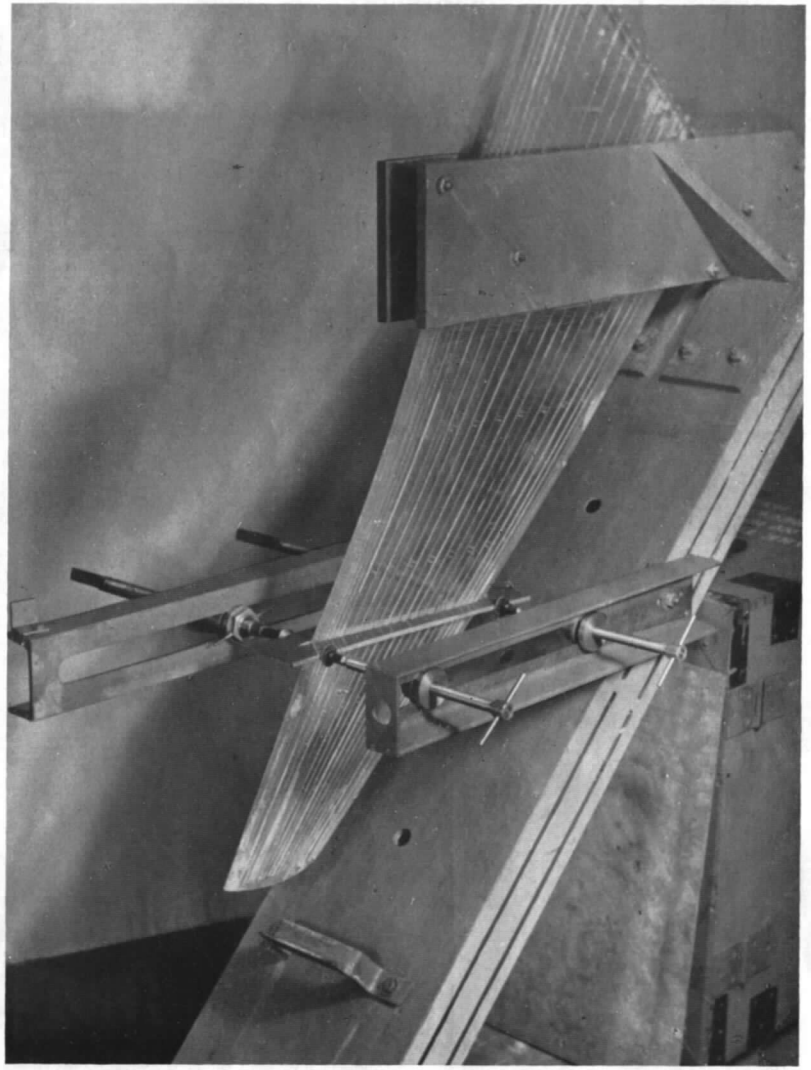

FIG. 4. The model undergoing deformation in the deforming frame.

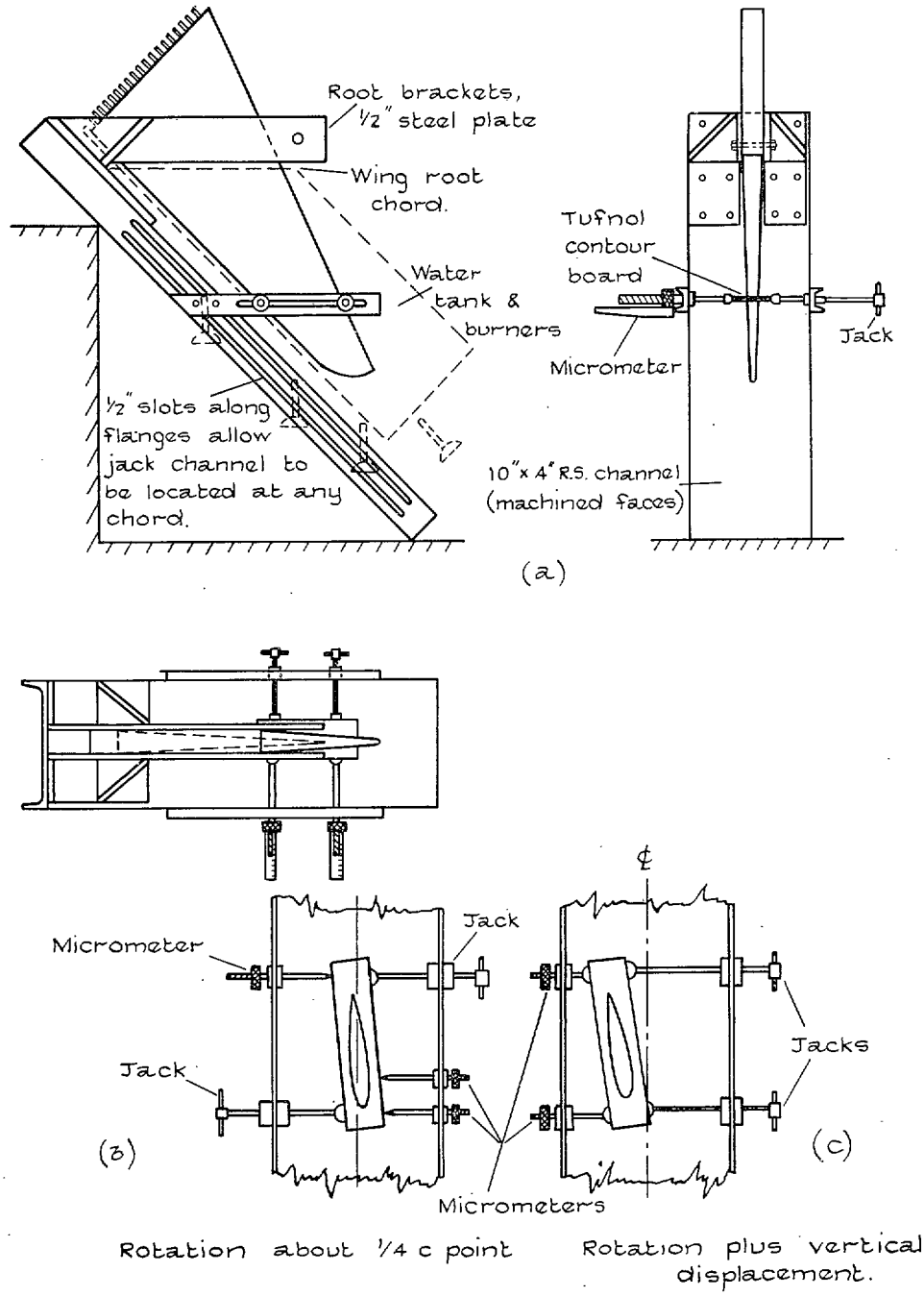

FIG. 5. Sketch of deforming frame.

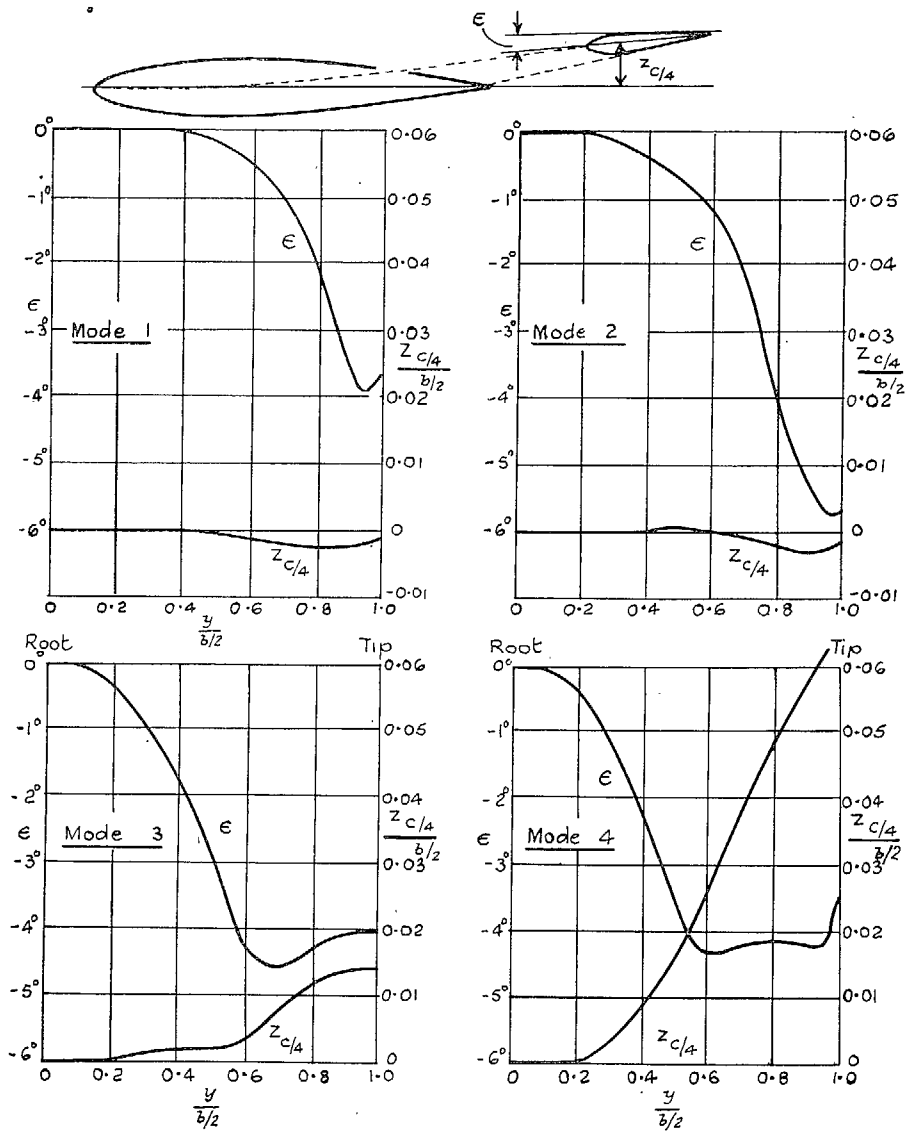

FIG. 6a. Angular rotation of chord and vertical displacement of quarter-chord line along span for various modes.

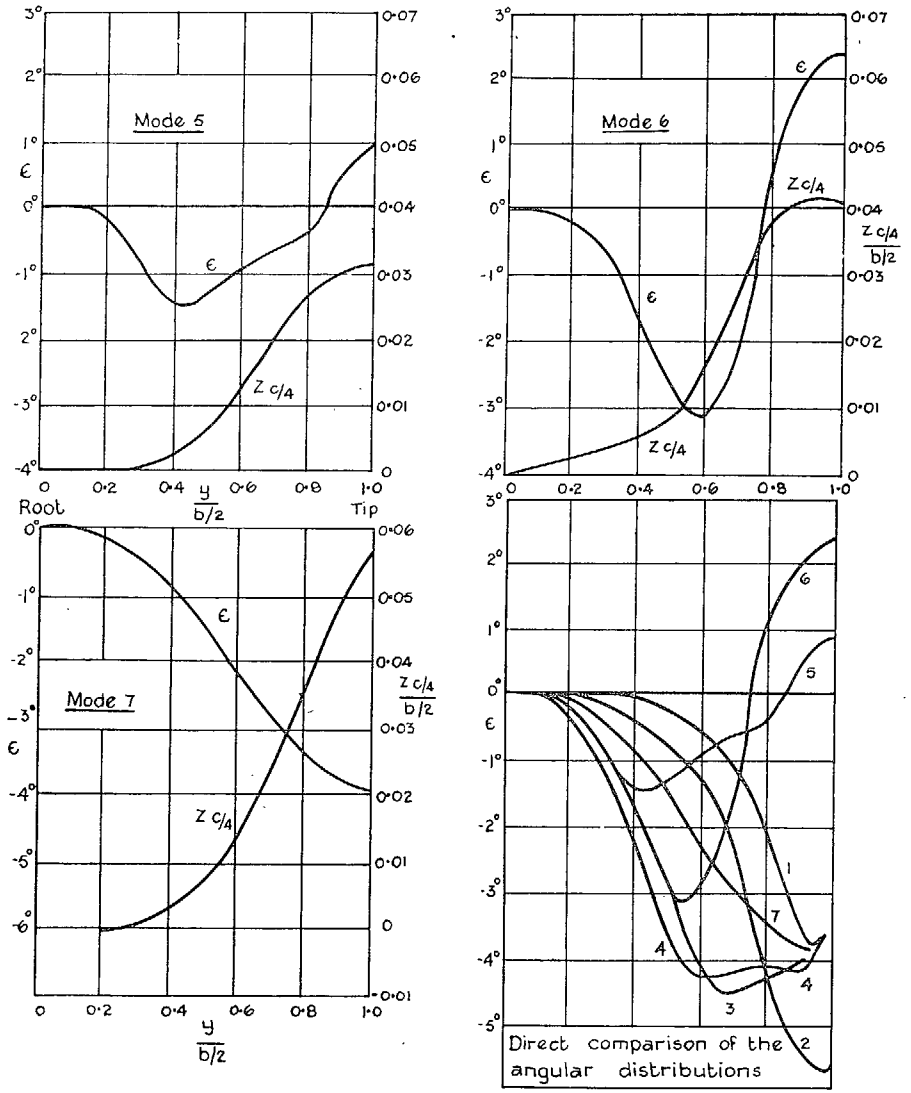

FIG. 6b. Angular rotation of chord and vertical displacement of quarter-chord line along span for various modes.

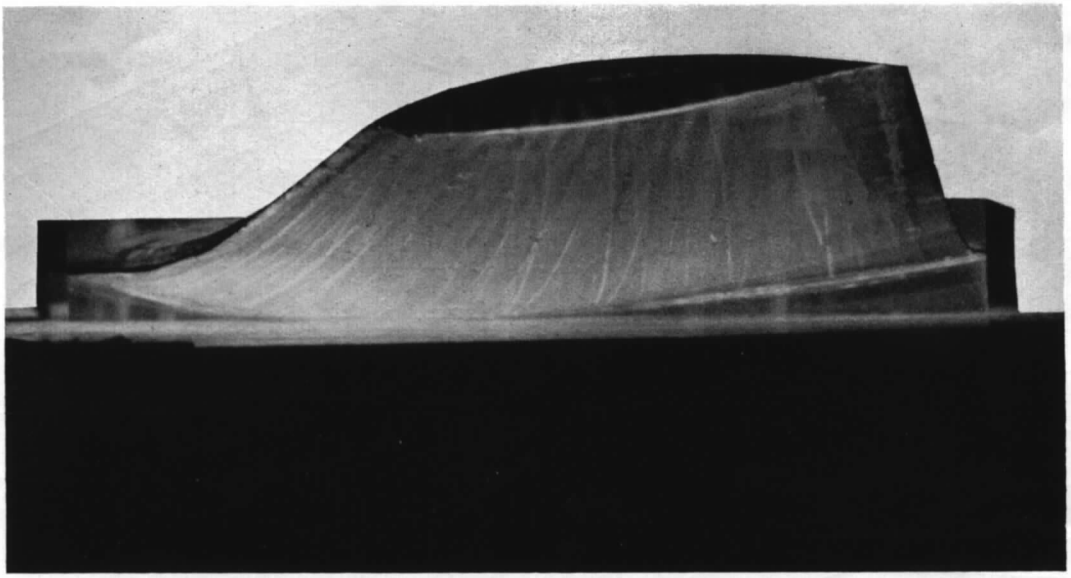

FIG. 7a. Looking along quarter-chord line from tip.

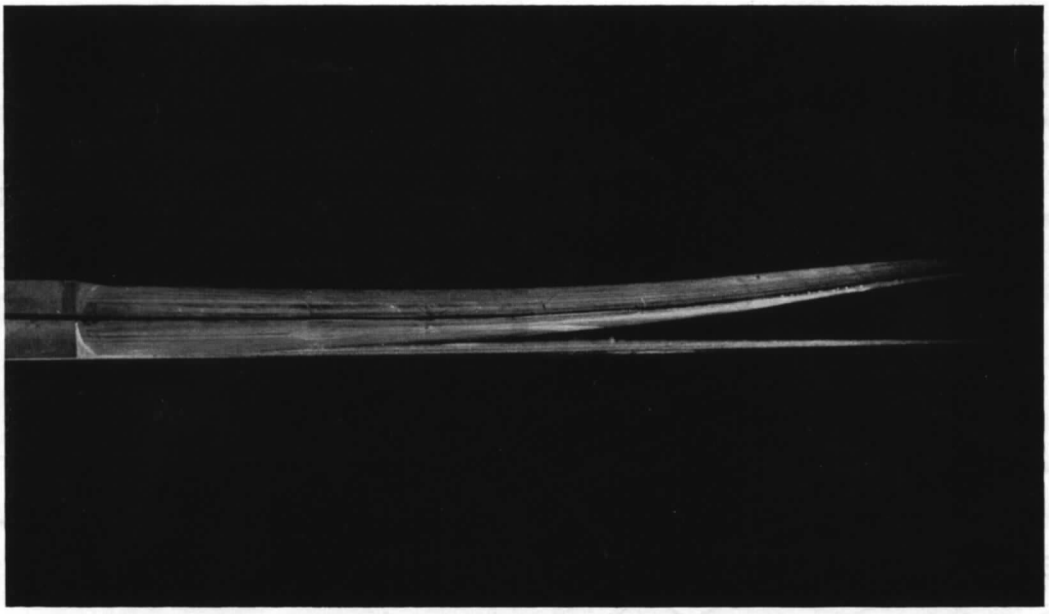

FIG. 7b. Looking at leading-edge, almost along line of flight.

Fig. 7. The wing deformed to have vertical upward displacement, and wash-out of incidence, towards the tip (Mode 7).

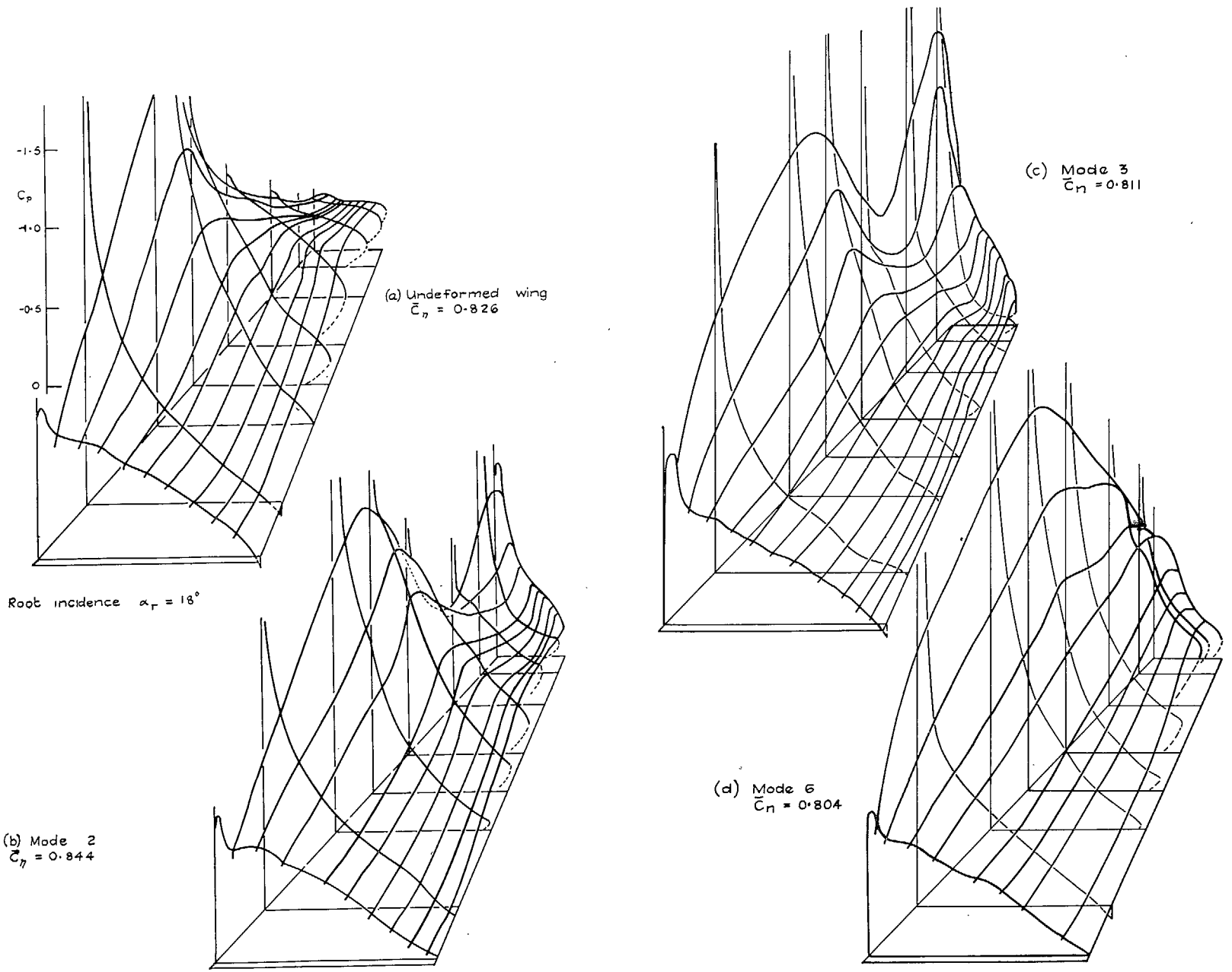

FIG. 8. Pressure distributions on the wing.

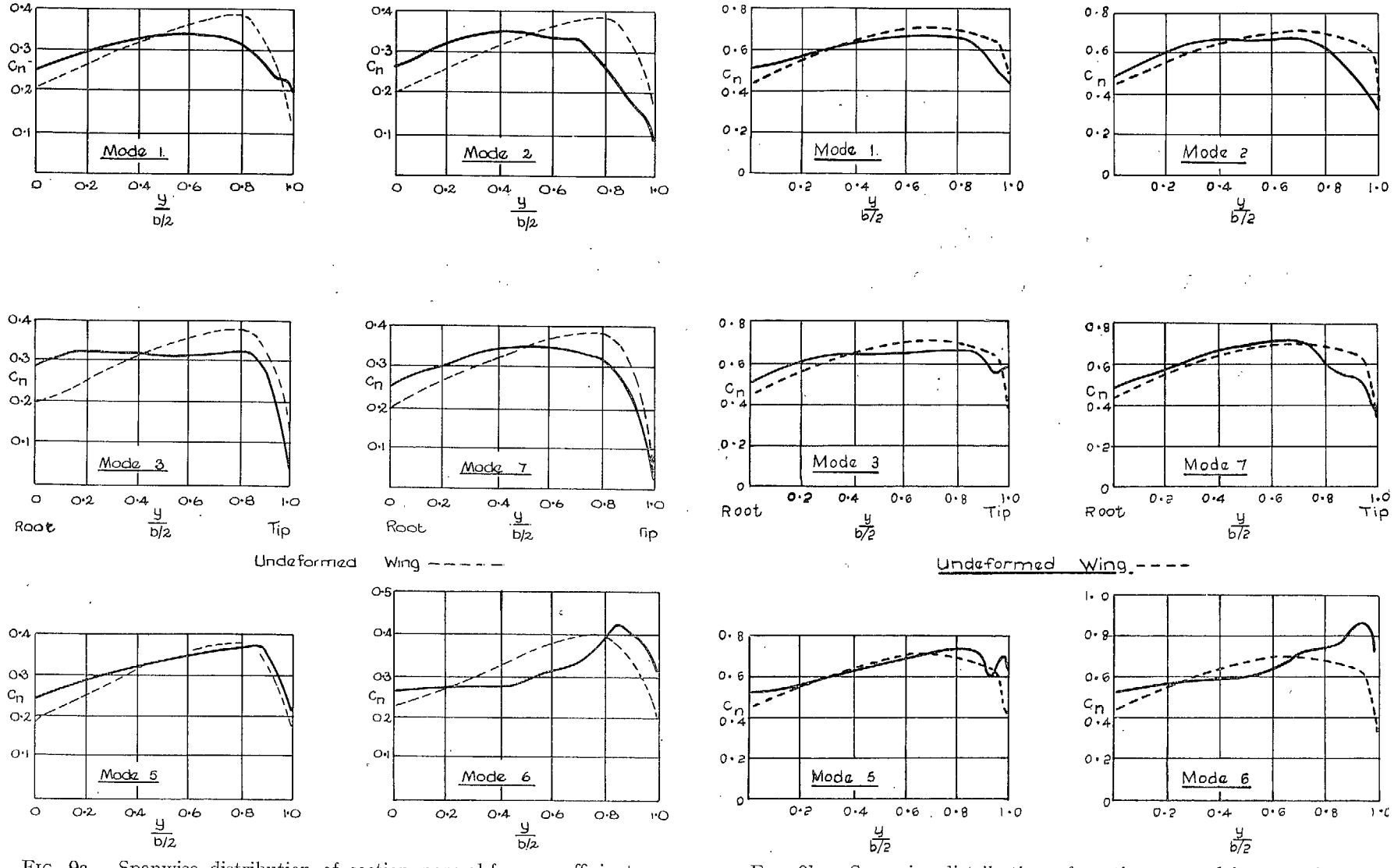

FIG. 9a. Spanwise distribution of section normal-force coefficient. $\bar{C}_n = 0{\cdot}297$.

FIG. 9b. Spanwise distribution of section normal-force coefficient. $\bar{C}_n = 0{\cdot}583$.

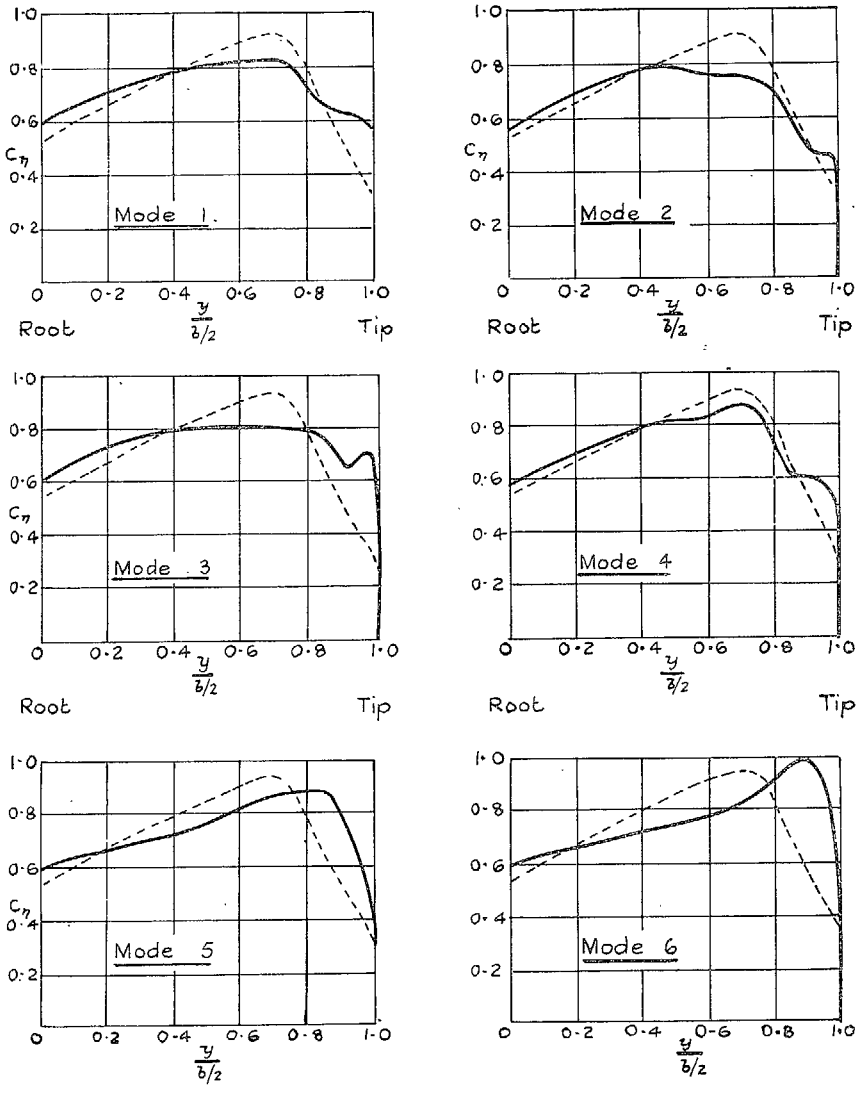

FIG 9c. Spanwise distribution of section normal-force coefficient. $\bar{C}_n = 0{\cdot}694$.

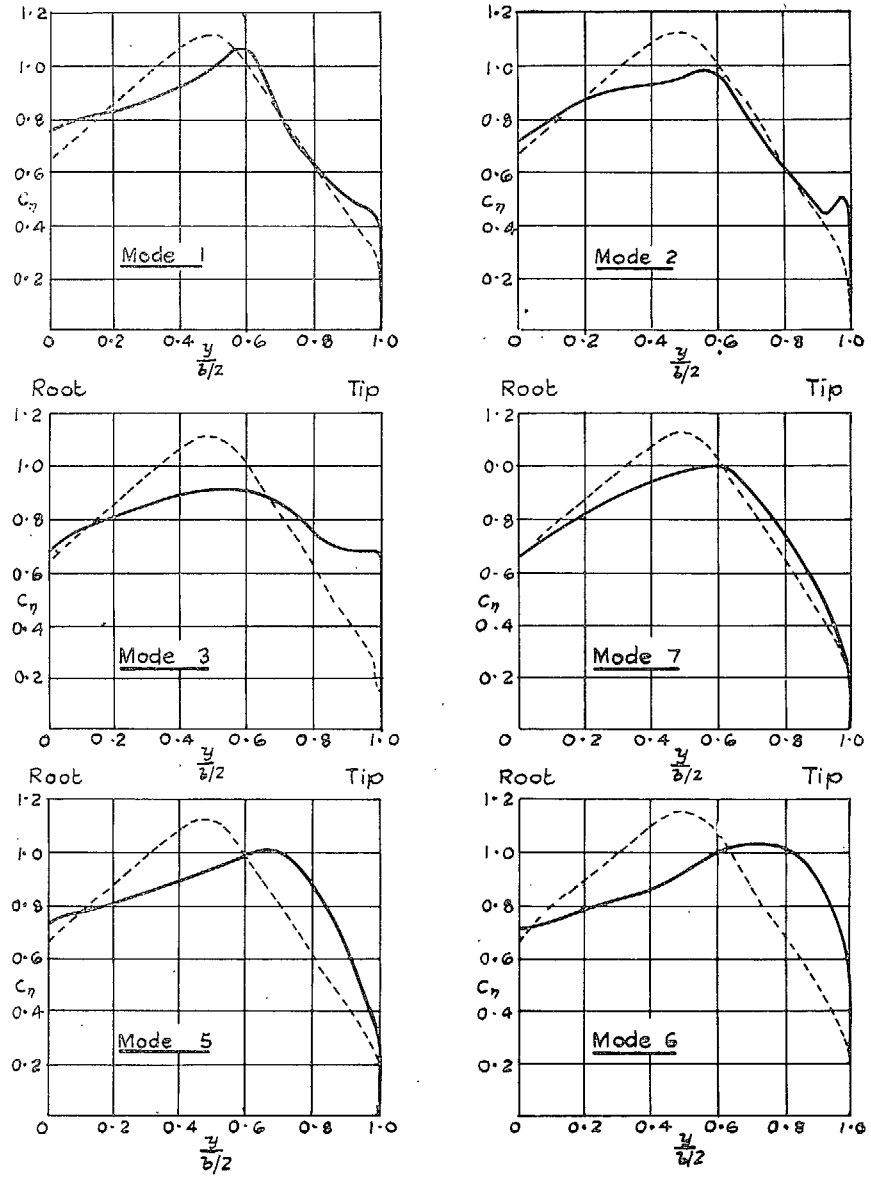

FIG. 9d. Spanwise distribution of section normal-force coefficient. $\bar{C}_n = 0{\cdot}82$.

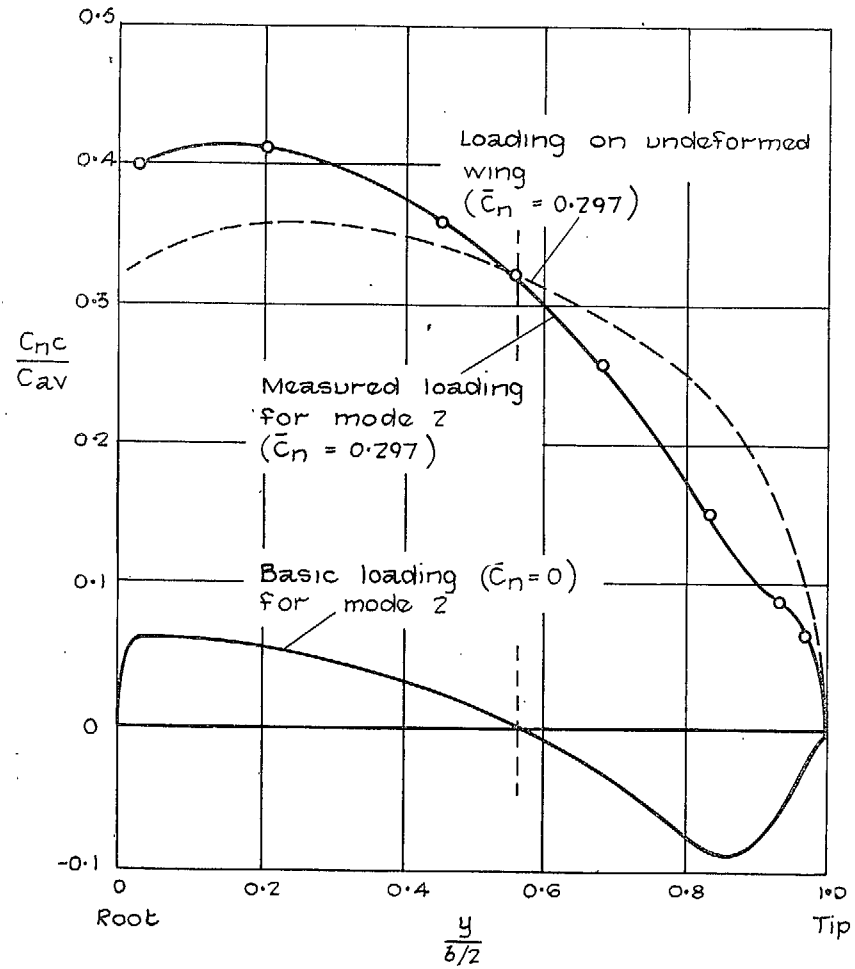

FIG. 10. The basic loading obtained by subtracting the additional loading from the total loading ($\bar{C}_n = 0{\cdot}297$).

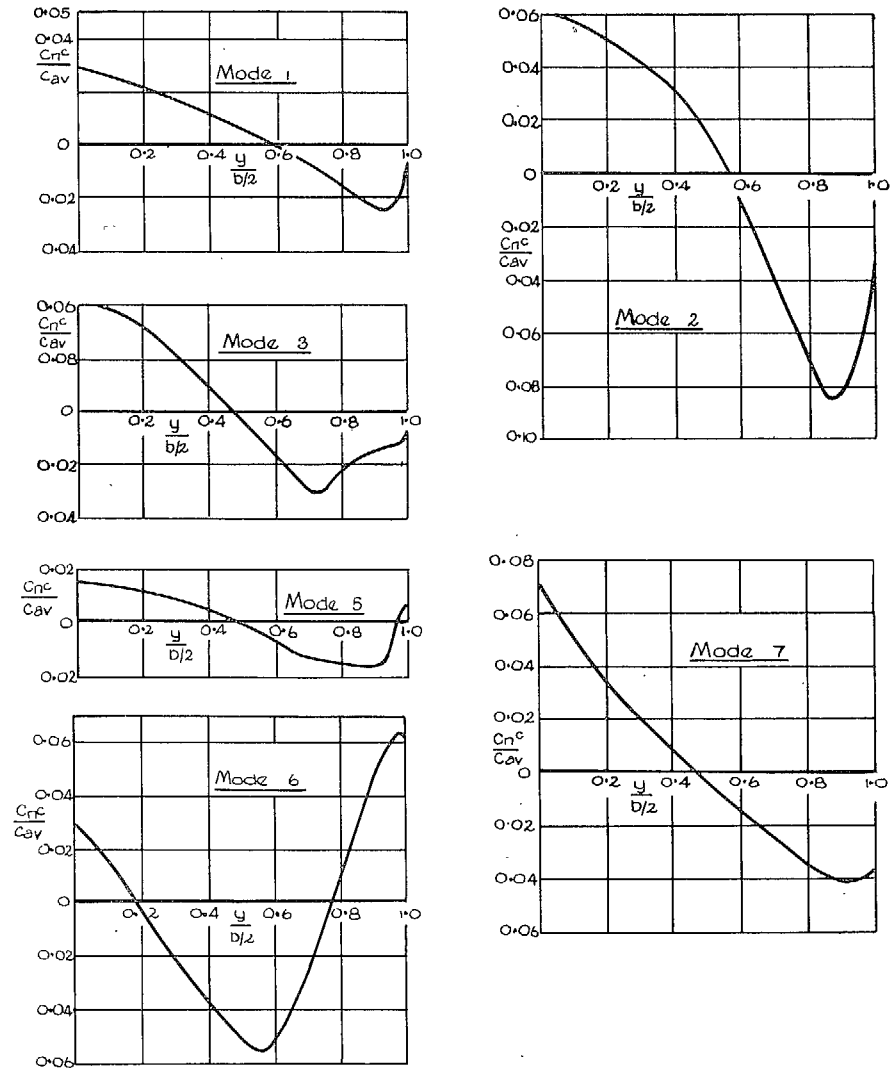

FIG. 11. Basic span loading for the various modes ($\bar{C}_n = 0$).

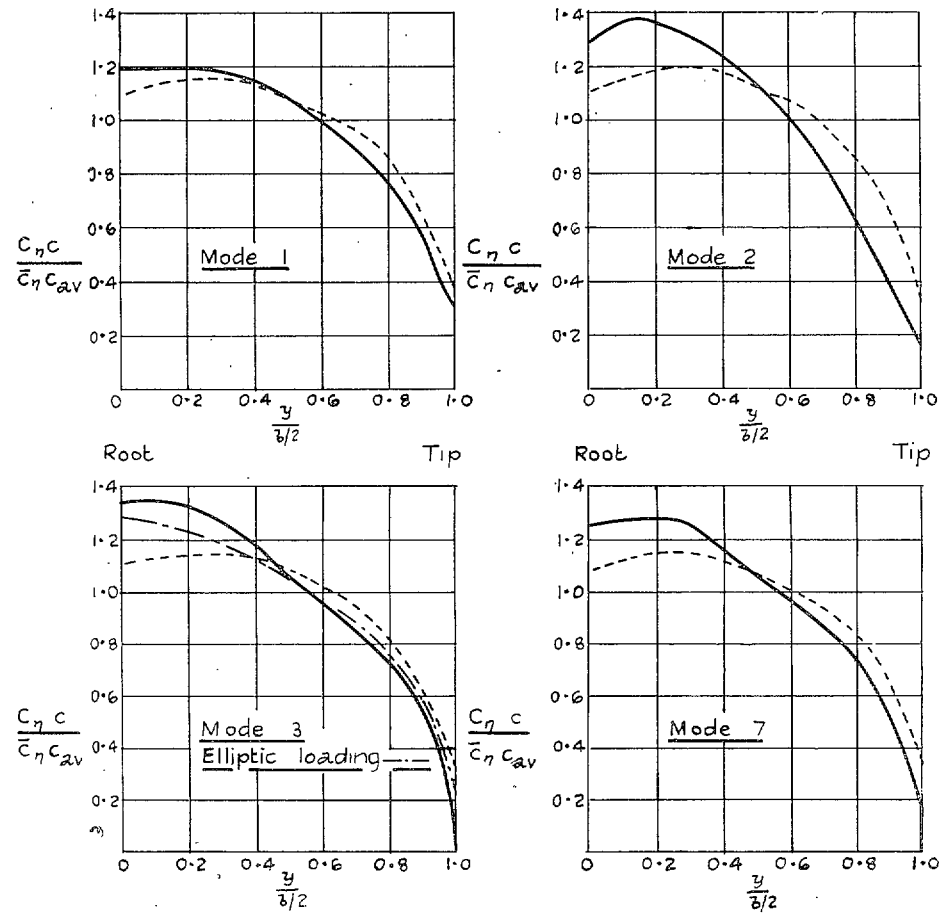

FIG. 12a. Comparison of span loading for various modes.

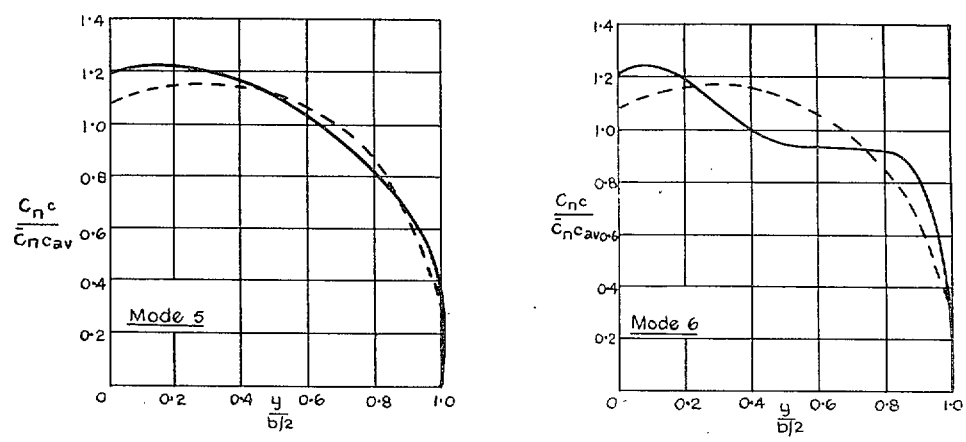

FIG. 12b. Comparison of span loading for various modes.

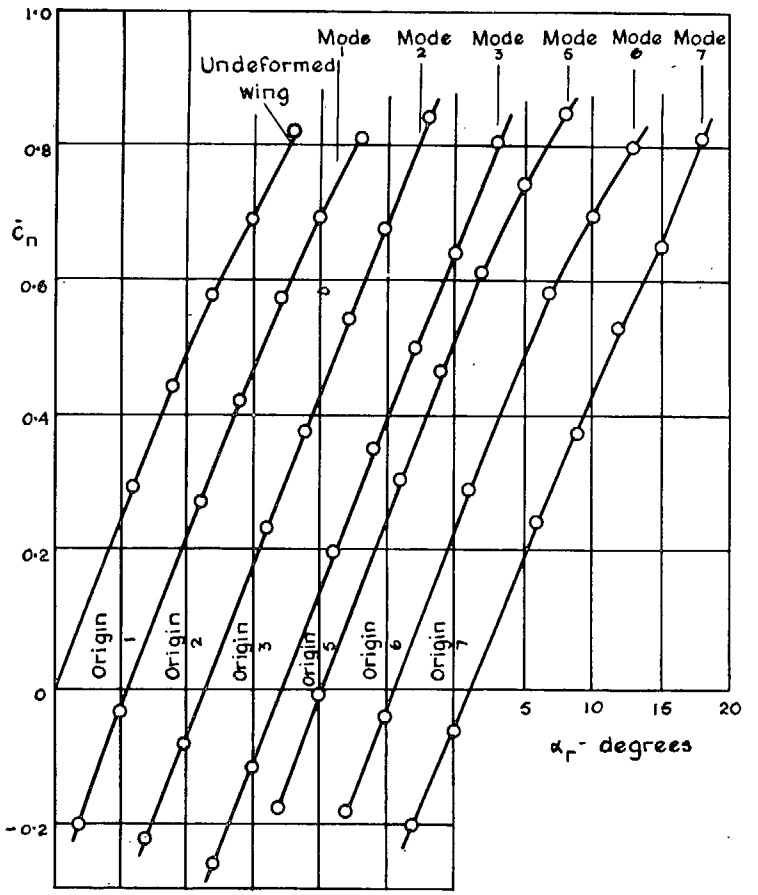

FIG. 13. Overall normal-force curves for the various modes.

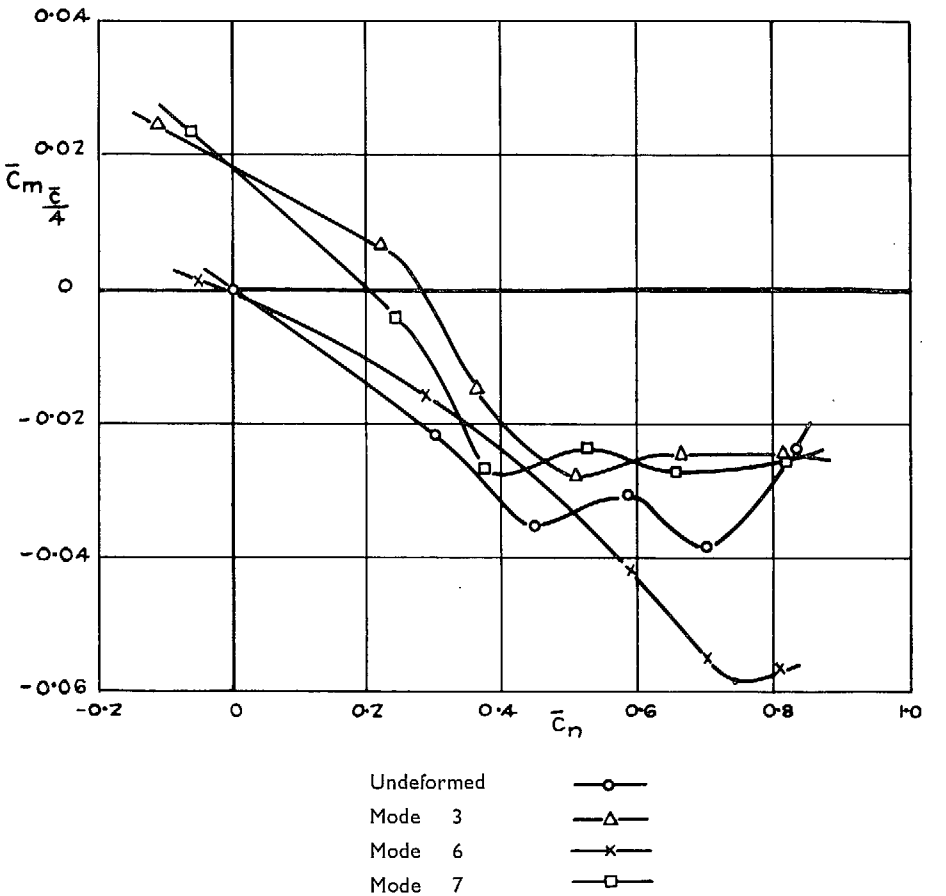

FIG. 14. Pitching-moment curves for various modes.

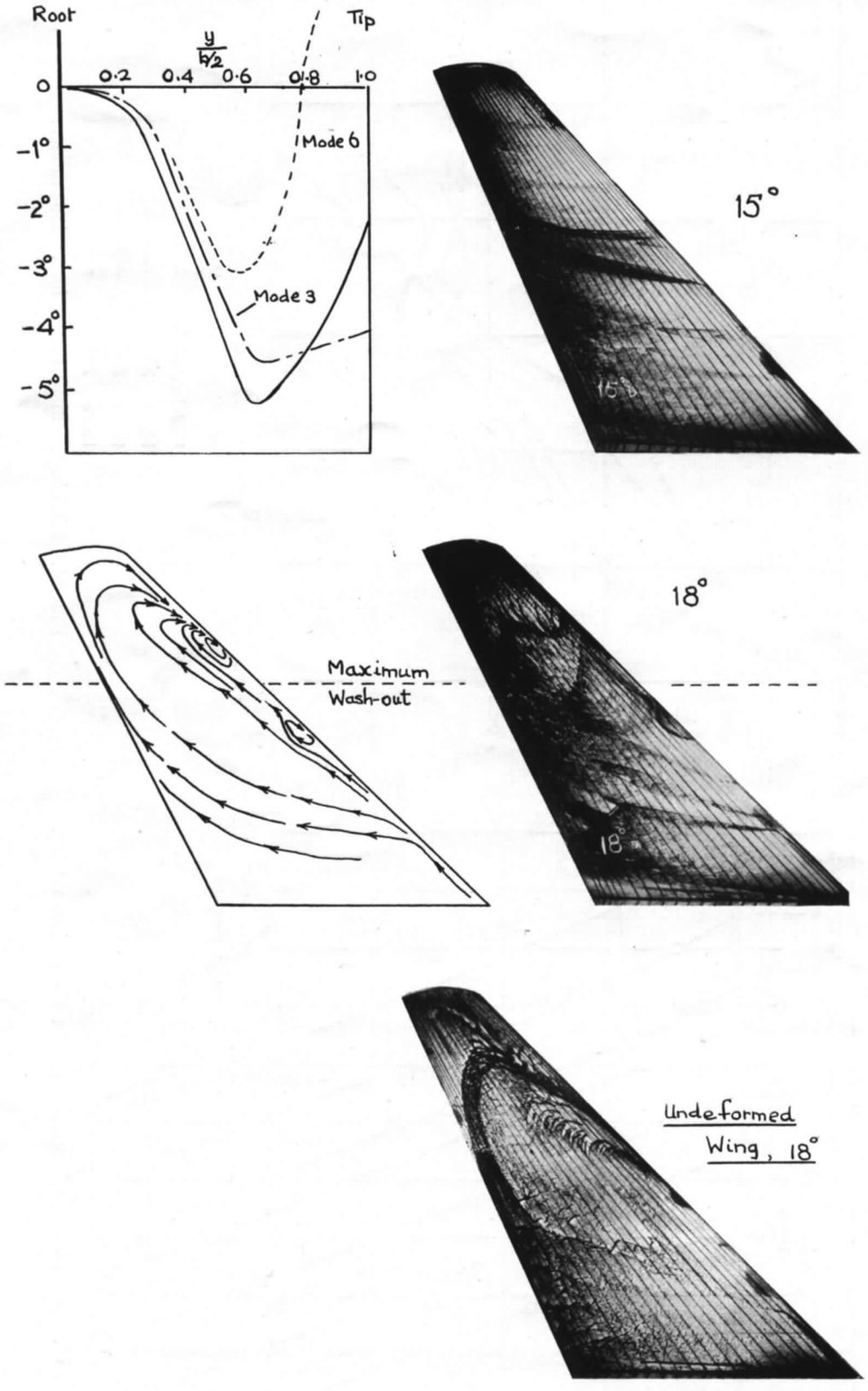

FIG. 15. Liquid-film patterns on the wing with the deformation shown.

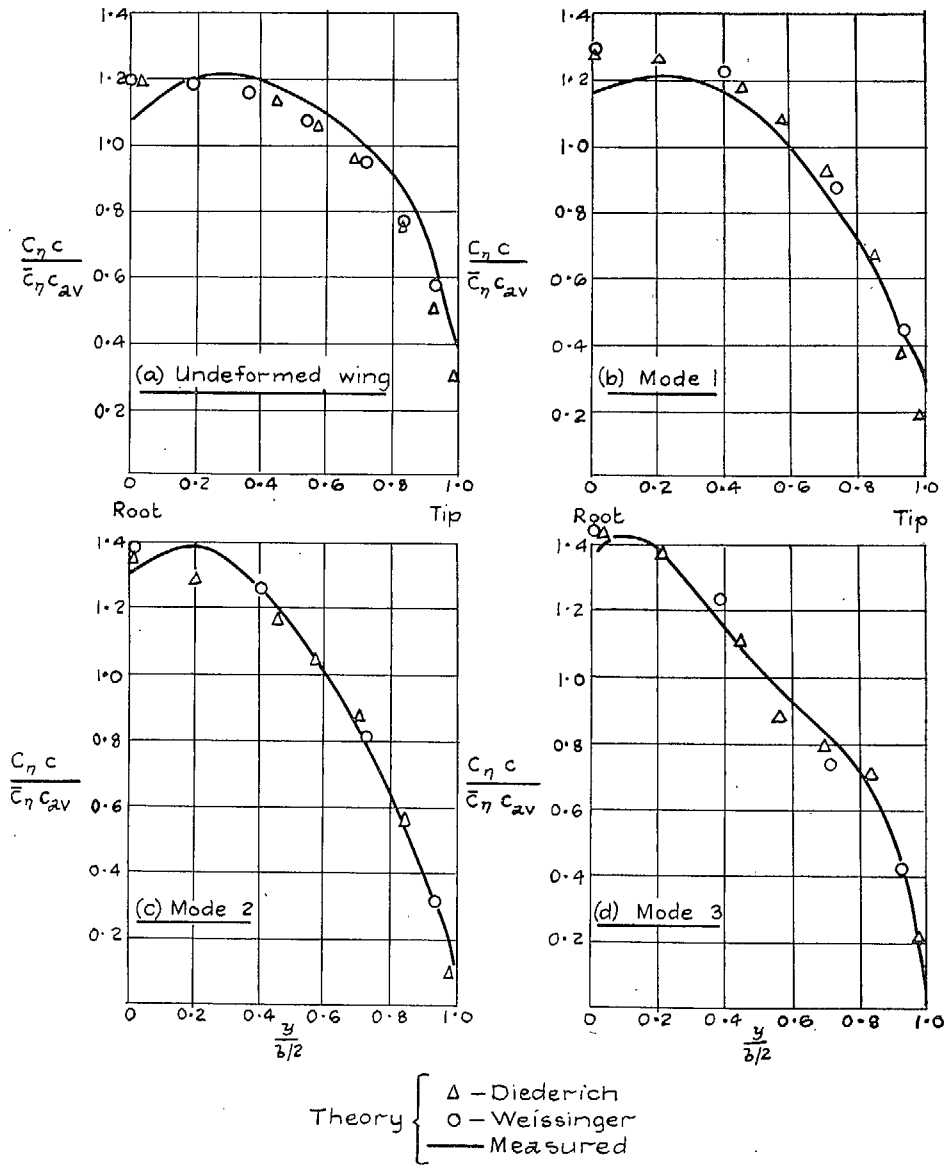

FIGS. 16a to 16d. Comparison of measured and calculated span loading.

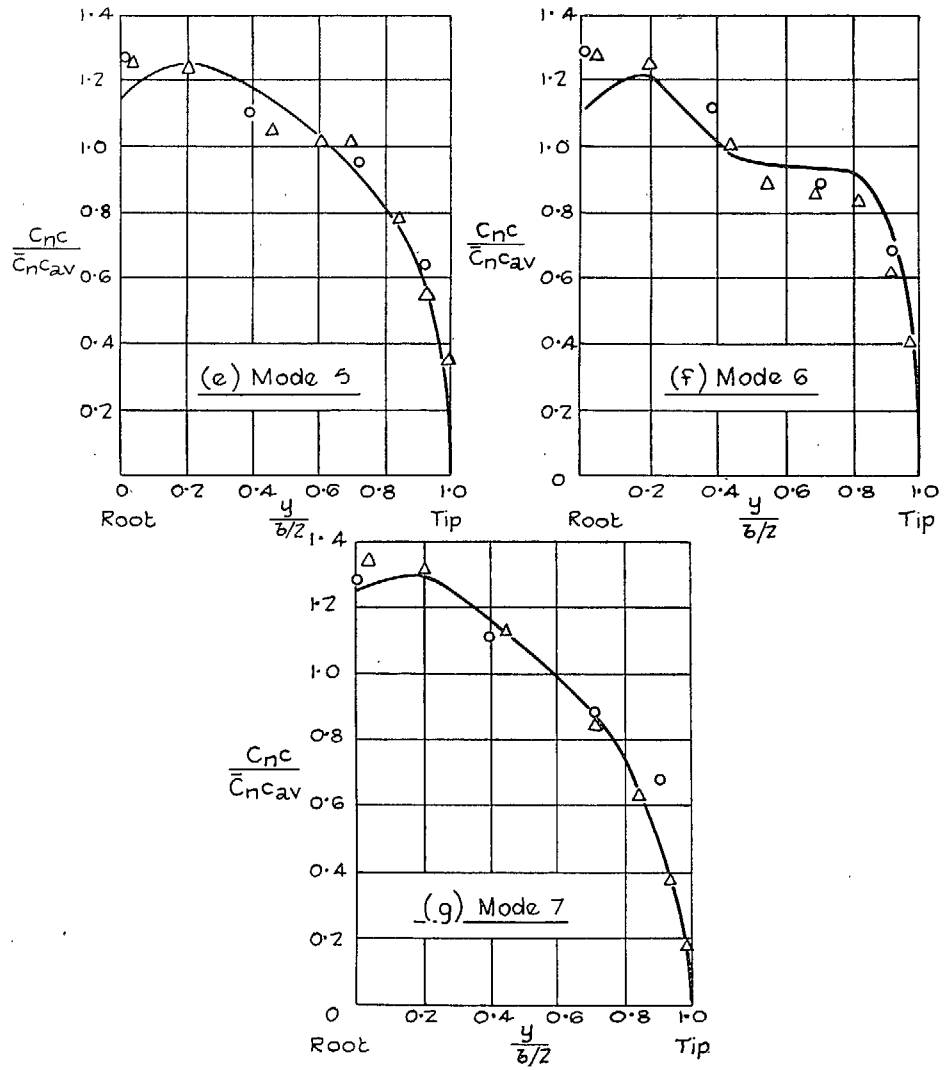

FIGS. 16e to 16g. Comparison of measured and calculated span loading.

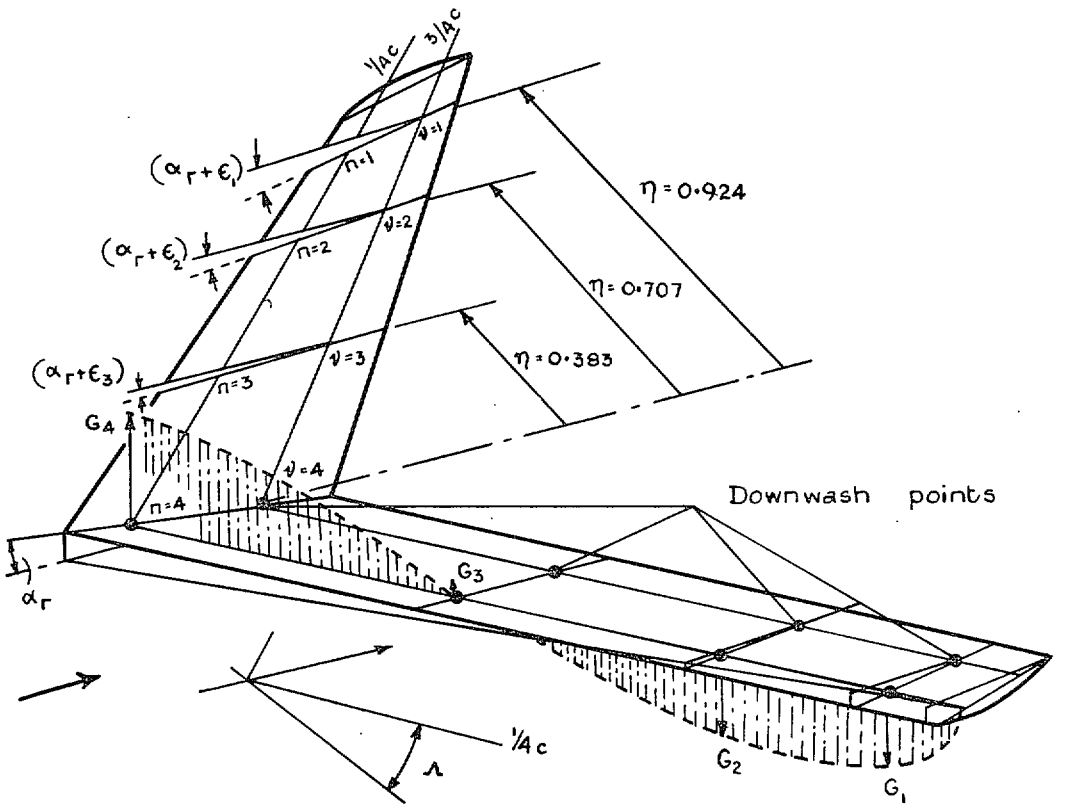

FIG. 17. Representation of swept wing for Weissinger loading theory (deformed wing).

(3923) Wt. 19/8411 K8 6/56 Hw.

Publications of the Aeronautical Research Council

ANNUAL TECHNICAL REPORTS OF THE AERONAUTICAL RESEARCH COUNCIL (BOUND VOLUMES)

1938 Vol. I. Aerodynamics General, Performance, Airscrews. 50*s* (51*s*. 8*d*.)
Vol. II. Stability and Control, Flutter, Structures, Seaplanes. Wind Tunnels, Materials. 30*s*. (31*s*. 8*d*.)

1939 Vol. I. Aerodynamics General, Performance, Airscrews, Engines. 50*s*. (51*s*. 8*d*.)
Vol. II. Stability and Control, Flutter and Vibration, Instruments, Structures, Seaplanes, etc. 63*s*. (64*s*. 8*d*.)

1940 Aero and Hydrodynamics, Aerofoils, Airscrews, Engines, Flutter, Icing, Stability and Control, Structures, and a miscellaneous section. 50*s*. (51*s*. 8*d*.)

1941 Aero and Hydrodynamics, Aerofoils, Airscrews, Engines, Flutter, Stability and Control, Structures. 63*s*. (64*s*. 8*d*.)

1942 Vol. I. Aero and Hydrodynamics, Aerofoils, Airscrews, Engines. 75*s*. (76*s*. 8*d*.)
Vol. II. Noise, Parachutes, Stability and Control, Structures, Vibration, Wind Tunnels. 47*s*. 6*d*. (49*s*. 2*d*.)

1943 Vol. I. Aerodynamics, Aerofoils, Airscrews. 80*s*. (81*s*. 8*d*.)
Vol. II. Engines, Flutter, Materials, Parachutes, Performance, Stability and Control, Structures. 90*s*. (91*s*. 11*d*.)

1944 Vol. I. Aero and Hydrodynamics, Aerofoils, Aircraft, Airscrews, Controls. 84*s*. (86*s*. 9*d*.)
Vol. II. Flutter and Vibration, Materials, Miscellaneous, Navigation, Parachutes, Performance, Plates and Panels, Stability, Structures, Test Equipment, Wind Tunnels. 84*s*. (86*s*. 9*d*.)

Annual Reports of the Aeronautical Research Council—

1933–34	1*s*. 6*d*. (1*s*. 8½*d*.)	1937	2*s*. (2*s*. 2½*d*.)
1934–35	1*s*. 6*d*. (1*s*. 8½*d*.)	1938	1*s*. 6*d*. (1*s*. 8½*d*.)
April 1, 1935 to Dec. 31, 1936	4*s*. (4*s*. 5½*d*.)	1939–48	3*s*. (3*s*. 3½*d*.)

Index to all Reports and Memoranda published in the Annual Technical Reports, and separately—

April, 1950 - - - - R. & M. No. 2600 2*s*. 6*d*. (2*s*. 7½*d*.)

Author Index to all Reports and Memoranda of the Aeronautical Research Council—

1909–January, 1954. R. & M. No. 2570 15*s*. (15*s* 5½*d*.)

Indexes to the Technical Reports of the Aeronautical Research Council—

December 1, 1936 — June 30, 1939	R. & M. No. 1850	1*s*. 3*d*. (1*s*. 4½*d*.)
July 1, 1939 — June 30, 1945	R. & M. No. 1950	1*s*. (1*s*. 1½*d*.)
July 1, 1945 — June 30, 1946	R. & M. No. 2050	1*s*. (1*s*. 1½*d*.)
July 1, 1946 — December 31, 1946	R. & M. No. 2150	1*s*. 3*d*. (1*s*. 4½*d*.)
January 1, 1947 — June 30, 1947	R. & M. No. 2250	1*s*. 3*d*. (1*s*. 4½*d*.)

Published Reports and Memoranda of the Aeronautical Research Council—

Between Nos. 2251–2349	R. & M. No. 2350	1*s*. 9*d*. (1*s*. 10½*d*.)
Between Nos. 2351–2449	R. & M. No. 2450	2*s*. (2*s*. 1½*d*.)
Between Nos. 2451–2549	R. & M. No. 2550	2*s*. 6*d*. (2*s*. 7½*d*.)
Between Nos. 2551–2649	R. & M. No. 2650	2*s*. 6*d*. (2*s*. 7½*d*.)

Prices in brackets include postage

HER MAJESTY'S STATIONERY OFFICE

York House, Kingsway, London W.C.2; 423 Oxford Street, London W.1 (Post Orders: P.O. Box 569, London S.E.1); 13a Castle Street, Edinburgh 2; 39 King Street, Manchester 2; 2 Edmund Street, Birmingham 3; 109 St. Mary Street, Cardiff; Tower Lane, Bristol, 1; 80 Chichester Street, Belfast, *or through any bookseller*

S.O. Code No. 23–2938